AN ABSTRACT OF THE THESIS OF

Matthew M. Dalon for the degree of Master of Ocean Engineering in Ocean Engineering presented on June 13, 2007.

Title: Analysis of Rip Current Embayments on the Oregon Coast

Abstract approved:

Merrick C. Haller

Understanding the past, present, and future behavior of our nation's shorelines is vital for sensible coastal management. Localized areas of erosion, termed "erosional hot spots", can shift the shoreline landward threatening coastal infrastructure (Kraus and Galgano, 2001; Stauble and Gravens, 2004; McNinch, 2004). One specific type of erosional hot spot that is capable of causing damage to coastal dunes, cliffs, and property is a rip current embayment (Komar and Rea, 1976; Komar, 1983; Komar et al., 1988; Thornton et al., 2007). These features are hypothesized to form when rip currents transport sand from the beach face to the offshore forming localized embayments (Komar 1971).

Due to the difficulty in obtaining bathymetric and hydrodynamic data for these features, they are not well understood. In the work reported here we take advantage of available extensive and synoptic topographic data to characterize the

morphology of plausible rip current embayments found along stretches of the Oregon coast. Following the quantification of rip current embayment morphology a numerical modeling study is performed to briefly investigate the nearshore hydrodynamics within a typical rip current embayment.

Lidar data along the Oregon coastline, collected in 1997, 1998, and 2002 (NOAA 2007a), provides high resolution topographic data for the analysis of the beach face morphology including rip current embayments. From these data, four continuous, sandy beach sections of the Oregon coastline were selected to be studied. A methodology based on these data is presented and is used to quantify and summarize the observed physical scales of rip current embayments using topographic data. Four morphologic characteristics are measured and tabulated for each embayment including length, amplitude, aspect ratio, and skewness. The number of embayments, embayment location, mean embayment location, and spacing at each study site are then compared.

A total of 98 embayments occupying 77% of the total study area were found within the study area. The embayments have lengths of O(100 m) and amplitudes of O(10 m) with an average length and amplitude of 591 and 18 meters, respectively. The embayment locations are random and widely distributed along the study sites.

Lidar data does not provide the hydrodynamic data needed to demonstrate that these morphologic features are directly formed by rip currents. Hence, a brief modeling study is also performed. The purpose of this effort is to assess whether it

is possible or likely that rip currents are generated within these morphologic features. In addition, we explore the sensitivity of rip existence to the expected wave conditions.

The model study utilizes the SHORECIRC circulation model, in conjunction with the REF/DIFF wave model. An idealized version of a rip current embayment that is based on the field data analysis is used as the input bathymetry for the model study. The model study demonstrates that rip currents are possible within the morphologic features we have identified. Results also indicated that the rip currents generated under the median wave condition, 2.0 meter wave height, were the strongest, suggesting that the middle of range of expected wave conditions may be the mode effective at generating rip currents and potentially rip embayments.

Analysis of Rip Current Embayments on the Oregon Coast

by

Matthew M. Dalon

A THESIS

submitted to

Oregon State University

in partial fulfillment of
the requirements for the
degree of

Master of Ocean Engineering

Presented June 13, 2007
Commencement June 2008

Master of Ocean Engineering thesis of Matthew M. Dalon

presented on June 13, 2007

APPROVED:

Major Professor, representing Ocean Engineering

Head of the Department of Civil, Construction, and Environmental Engineering

---

Dean of the Graduate School

I understand that my thesis will become part of the permanent collection of Oregon State University libraries. My signature below authorizes release of my thesis to any reader upon request.

Matthew M. Dalon, Author

ACKNOWLEDGEMENTS

I would first like to thank my advisor Merrick Haller for providing this research opportunity. He was always there to pick me up when I was down and keep me on the right path. I would also like to thank my other committee members; Tuba Ozkan-Haller, Peter Ruggiero, and Roger Graham. Together this committee provides great advice and insight into my research. The ability to add a modeling study to this research is due to Greg Wilson (Canadian Greg) who solved all my SHORECIRC problems. Another big part of my success at OSU is owed to Pato who always managed to kindly assist me in my day to day obstacles. Most importantly, I would like to thank my friends and family that have supported me thought this two year endeavor. Without all of your love this would have proved a more difficult task.

This research was supported by the National Sea Grant College Program of the U.S. Department of Commerce's National Oceanic and Atmospheric Administration under NOAA grant number NA06OAR4170010 (project number R/CNH07) and by appropriations made by the Oregon State legislature. The views expressed herein do not necessarily reflect the views of any of those organizations.

TABLE OF CONTENTS

TABLE OF CONTENTS (Continued)

TABLE OF CONTENTS (Continued)

LIST OF FIGURES

LIST OF FIGURES (Continued)

LIST OF TABLES

LIST OF APPENDIX

LIST OF APPENDIX TABLES

Analysis of Rip Current Embayments on the Oregon Coast

1. Introduction

The sandy shores of Oregon are seldom straight. Dynamic in nature, their shape and form is constantly shifting. The historical, present, and future location of the shoreline is vital to a variety of coastal engineering applications. Understanding the overall shoreline change is further complicated by longshore variability within the shoreline. In order to understand the variability of our beaches they must be measured and analyzed.

Longshore variability of the shoreline can be partially attributed to longshore gradients in sediment flux. The forcing of sediment flux gradients along beaches is not well understood for relatively small length scales O(1km) and is difficult to measure. However, the features resulting from these gradients are apparent on the beachface and are readily accessible.

Gradients in sediment flux can occur over various spatial and temporal scales and cause both erosion and accretion of the shoreline. Within a relatively straight and stable shoreline a local gradient in sediment transport can cause a localized area of erosion. The resulting erosional features are termed “hot spots” and can occur on beaches with a positive, zero, or negative net rate of shoreline change (Kraus and Galgano, 2001; Stauble and Gravens, 2004; McNinch, 2004).

A total of 18 types of erosional hot spots and their respective causes have been identified (Kraus and Galgano, 2001). Each erosional hot spot has an

associated cause controlling its spatial and temporal scales which are often directly linked (List et al., 2005). Within a stretch of beach there may be one or more types of erosional hot spots present. The resulting shoreline variability encompasses a broad range of length scales. These features range from small beach cusps O (10 m) to large regions of erosion O (10 km). The summation of these features creates the irregular shorelines common throughout the world. Though hotspots have been classified, we do not have a complete enough understanding of their formation and evolution to make predictions.

This study will concentrate its focus on a singe type of erosional hot spot, the rip current embayment. Rip current embayments are cuspate features within the shoreline caused by a localized area of erosion (Komar, 1971; Thornton et al. 2007). Observations of these embayments suggest typical alongshore length scale of O(100's meters) of affected shoreline and an associated cross-shore amplitude length scale of O(10's meters) of affected beach width (Cook, 1970; Dolan, 1971; Komar, 1971; Komar and Rea, 1976; Komar et al., 1988; Revell et al., 2003; Allan et al., 2003; Shand et al., 2004; Thronton et al., 2007). The alongshore limits of rip embayments is where the local shoreline deviates from the overall shoreline. These endpoints of the embayments are termed cusps or horns. These horns are typically erosional remnants but can also be depositional and are more defined when embayments are adjacent to one another (Komar, 1971). The endpoints of isolated embayments are less defined.

It has been historically hypothesized that embayments form in the lee of rip current channels (Shepard et al., 1941; Komar, 1971). This correlation was recently confirmed by Thornton et al. (2007) for rip embayments in California. They found that the location of embayments had a direct correlation with the locations of rip current channels. Therefore the location of rip currents is critical to the formation and location of these embayments. Thus it is necessary to understand rip currents in order to further our understanding of rip embayments.

Rip currents are relatively narrow seaward flowing jets of water that are formed within the surf zone and extend beyond the surfzone. The rip current is part of a larger circulation cell that is caused by gradients of radiation stress within the surf zone. Longshore gradients of wave heights and radiation stress are caused by nearshore morphology or wave hydrodynamics, or a combination of both. There are two important effects of rip currents pertinent to this research; their effects on both sediment transport and wave breaking. Large concentrations of sediment are often observed within rip currents. This sediment is excavated from feeder channels, rip channels (Aagaard et al., 1997), and, in our case, the shoreline; however, the relative quantities are unknown. The excavation of rip current channels has a direct effect on wave breaking. The deeper waters of the channel allow waves to propagate further shoreward. This shoreward propagation of energy is thought to be critical in the development of rip embayments.

The location and persistence of rip currents is not well known (Holman et al., 2006) and has a direct relationship to the location and persistence of

embayments. Rip currents on open coasts appear at random locations unless controlled by permanent morphologic features conducive to rip generation. If rip currents are able to create a rip channel the location of rip currents is no longer random and is controlled by the rip channels (Murray, 2004). Along a beach multiple rip currents may exist, varying in size and strength. Because of this, multiple embayments can be found within a continuous beach. Observations in California revealed continuous rip embayments with a relatively narrow common alongshore lengths of O(200 meters) on a single beach (Thornton et al., 2007). In Oregon, the embayments have a broader range of length scales (Komar, 1971 Komar and Rea, 1976; Komar et al., 1988). This is due to varied size and strengths of rip currents creating a range of embayments sizes accounting for the irregular shoreline (Komar, 1983).

The temporal scale of rip embayments is not clearly defined. It is believed that the temporal scale is highly dependant upon the wave forcing. Wave forcing is highly variable throughout the world and thus the temporal scale is dependant upon location. Shand et al. (2004) observed three rip embayments in New Zealand to have a duration ranging from 4-8 weeks. Anecdotal observations of rip current embayments in Oregon suggest these features can persist for months but they have not been observed to last over a year's time.

A rip embayments' life cycle is composed of generation, persistence, and extinction. Generation has been difficult to capture due to the random location of rip currents and hence, rip embayments. It is believed that the generation is

dependant upon rip current strength and persistence however these thresholds are unknown. Once formed it may persist without an active rip current. Rip current embayments with length scales of O(200 meters) have been observed to persist under spring tides and mean wave heights of 2.2 meters (Shand et al., 2004). Embayments are not static, the can grow, change shape, and migrate. Migration rates have been observed on O(m/day) (Komar et al., 1989; Thornton et al., 2007).

Rip current embayments are eradicated from the shoreline through infilling which can occur in two separate conditions; high wave energy and low wave energy. During high energy storm events beaches tend to erase morphology forming flat beaches with linear off-shore bars, and the rip channels and embayments are filled in during these conditions. This type of infilling is similar to 'reset' events that eliminate rip channel bathymetry (Holman et al., 2006). Conversely, low energy events, with small long swell, can fill in the embayments (Thornton et al., 2007). The thresholds for these separate conditions are unknown.

1.1. Effects of Rip Current Embayments

Rip embayments are frequently an important cause to coastal erosion problems. They can have a direct effect on beach, dune, and cliff erosion by affecting the beaches ability to act as a buffer during energetic conditions. The embayment itself is not a highly erosive feature, however; the erosion they facilitate is (Komar, 1983). Excavation of the embayment shifts the shoreline landward and reduces beach width O (10m). Additionally, embayments are coupled with relatively deeper water within the surfzone. During elevated water

levels and energetic storm events, less wave energy is dissipated in the surf; hence more energy reaches the shoreline of the embayments as compared to the adjacent beach. Wave energy transmitted through a reduced beach width can attack coastal dunes and bluffs more directly. These features are easily eroded, therefore rip current embayments can be responsible for large episodic erosion within the dune and cliff systems (Komar and Rea, 1976; Komar, 1983; Komar et al., 1988; Thornton et al., 2007).

The effect of rip current embayments is dependant upon beach state. The overall beach state can be related to the beach width. The difference between erosional rates due to storm frequency and the accretion rates due to low energy conditions necessary to rebuild the beach governs the beach width. In a region where the rate of erosion caused by storm frequency exceeds the beach recovery rate the overall erosion is amplified, especially where there is a limited sand supply (Morton et al., 1995). When embayments form on a beach that has an overall narrow beach width the potential for the embayments to facilitate dune and bluff erosion is increased.

Dunes and bluffs provide protection for infrastructure of coastal properties. Whereas shorelines can recover rapidly from hot spot erosion (List et al., 2005), dune and bluff erosion scar the beach system. Cliffs cannot recover from an erosion event; there is not a natural way for it to build seaward. Dune erosion is recoverable, but is a relatively slow process. Dunes recover from erosion with an

initial slumping of the scarped dune within the region of erosion. They are then built by aeolian transport (Rogers and Nash, 2003).

1.2. History of Rip Current Embayment Observations

1.2.1. Field Observations in Oregon

Rip embayments are a common feature along the Oregon coastline. However, there is limited published documentation regarding the morphological characteristics of rip current embayments. Often the amount of damage to the coastal system by rip embayments is related to the amount of dune/cliff recession and the affected dune length. A summary of documented damage caused by rip current embayments in Oregon is provided below.

The earliest example, provided by Komar and Rea (1976) of a rip embayment causing severe property damage occurred on the Siletz Spit located on the central Oregon coast. During the winter of 1972-73 a large rip current embayment formed and remained in a stationary location throughout the winter. The reduced width and deep water of the embayment coupled with spring tides and set-up from the winter swell allowed the swash to reach and remove the dune sand. Over a three week period of winter swell the maximum dune recession was 30 meters along a 650 meter stretch of central Siletz Spit. A house in construction was lost to the sea. Nearby homeowners recognized the impending threat and placed riprap fronting their property.

Rip current embayments have also been observed at Netarts Spit, Oregon, by Komar et al. (1989). At any given time their effect was local, only attacking 200-500 meters of dune length of the 6 km spit due to their random location. From aerial photography it was apparent that limited dune erosion was caused by rip current embayments over the years due to ample beach width. The beach width of the spit was reduced during the El Niño winter of 1982-83. The extreme southern storm track caused a large migration of sand northward leaving the southern portion of the beach thin and this section did not recover its width in subsequent years. With a narrow beach, the dune was left vulnerable to erosion within embayments and this proved problematic during ensuing years. Rip currents were often positioned offshore of the beach at Cape Lookout State Park, attacking dunes and a man-made bulkhead. This bulkhead came under severe attack in the winter of 1987-88 when again a major rip current was positioned offshore of the wall. From that winter to the next spring the rip current migrated northward, and correspondingly, the area of maximum erosion migrated north. By spring, little of the beach and bulkhead remained due to the rip current embayment and dune retreat had amounted to about 20 to 25 meters. A survey of this area was conducted and the location of the rip current embayment erosion was evident from a distinct topographic low.

A more recent example of the damaging effects of a rip embayment was observed by Jonathan Allan (pers. comm.) at Gleneden beach November 2006. Over a weekend ~3-5 meters of localized bluff erosion occurred due to the

presence of a rip current embayment. Emergency rip rap was placed to prevent any further erosion of the bluff and possible undermining of two household foundations. On the beach face the embayment created a ~1 meter scarp along the embayment. After the storm passed calm conditions persisted. It was observed that the embayment recovered similar to the reversing hotspots described by List et al. (2005). Unfortunately there were not any detailed measurements made during this event.

1.2.2. Laboratory and Modeling Observations

There have been limited laboratory and modeling studies of rip current embayments. Rip currents have been studied however the resulting beach face morphology is less examined. Field measurements of the morphology of rip current embayments and their associated hydrodynamics are difficult to obtain. Without knowledge of the offshore bathymetry there has been limited laboratory and modeling investigations.

Only two laboratory experiments investigating rip current embayments have been conducted by Komar (1971). The first experiment was conducted in 1968 in a 15.2 by 18.3 meter wave basin. An initial flat uniform sloping beach profile consisting of fine quartz sand was subjected to waves with a period of 3.24 sec for periods of 10 and 15 minutes. Four strong rip currents were produced and a cuspate shoreline was generated. In this study the locations of the embayments did not correlate with the locations of the rip current, instead the locations of the

horns corresponded with the location of the rip currents. This indicted deposition in the head of the rip neck.

The second experiment was conducted in a 16.2 by 58.0 meter wave basin. An initial flat uniform beach profile (1:12) consisting of smooth granular coal (0.8 mm) was subjected to wave periods and heights of 1.46 seconds and 5.6 cm. Permanent cuspate features formed again with the location of the embayment not corresponding to the location of rip currents.

In both of Komar's experiments the rip currents were depositional at the shoreward extent of the rip. Similar deposits at the convergence of feeder channels and base of the rip-neck channel have been observed in the field (Brander and Cowell, 2003). This type of deposition may explain the infilling of embayments. Formation of an embayment is dependent upon the ratio of sand deposited versus sand excavated and carried offshore at the base of the rip channel (Komar, 1971).

The author has no prior knowledge of attempts to model the hydrodynamics within a rip current embayment. On the other hand, rip currents have thoroughly been modeled and studied. It has been hypothesized that the hydrodynamics within rip embayments result in strong radiation stressgradients caused by the three dimensional morphology of rip embayments (Shand et al., 2004). The hydrodynamics are critical to the existence of these features.

1.3. Research Focus

Measurement of multiple rip embayments morphodynamics have not been collected and analyzed in Oregon. The motivation of this research is to use available large scale surveys to measure the morphological characteristics of rip current embayments in Oregon.

In order to better understand large scale beach behavior surveying systems have evolved considerably. Advances in Global Positioning System (GPS) and Light Detection and Ranging (lidar) technology have dramatically increased survey areas while decreasing survey time. These advanced surveying techniques provide a vertical accuracy similar to the average footprint depression (~15 cm) made in the sand by a human (Sallenger et al., 2003). The availability of this dense and accurate data allows more detailed studies of large areas previously unattainable.

First a method is developed to identify rip embayments from lidar data. Once the embayments have been identified and measured our objective is to resolve dominant feature signals. If found, these signals can provide valuable information regarding the behavior of rip current embayments on the Oregon coastline eventually leading to an understanding of the formation, evolution, and affects of rip current embayments.

With knowledge gained from the lidar results, the hydrodynamics within embayments is investigated. Rip embayment bathymetry is difficult to collect and thus not readily available. An ideal bathymetry is created using the average

morphology of measured embayments and the circulation patterns are modeled using SHORECIRC. From this modeling effort two major questions are investigated: do rip currents exist within embayments and if present, is there a threshold for rip current embayments.

This thesis is organized into two major sections. First morphological features consistent with rip current embayments are identified and measured at four study sites using lidar data collected in 1997, 1998 and 2002. From the results of the lidar analysis, an idealized rip current morphology is created and circulation within this feature is modeled using SHORECIRC.

2. Lidar Study Site and Data

This study focuses its attention to the beaches of the Oregon coastline. To analyze the characteristics of rip embayments in Oregon four study sites of continuous sandy beach were selected. These locations are named the Nehalem sub-cell, Rockaway sub-cell, Netarts sub-cell, and Siletz sub-cell. These locations were selected due to rip current embayment observations from historical documentation (Komar and Rea, 1976; Komar et al., 1989; Allan et al., 2003) and anecdotal observations. Before the specifics of the study site are described, a summary of the Oregon coastal conditions are presented.

2.1. Oregon Coastal Conditions

Oregon is located in the Pacific Northwest of the United States. Its coastline stretches 583 km from the California border north to Astoria and the mouth of the Columbia River. Of the 583 km of coastline 422 km are composed of sand beaches backed by dunes or bluffs. The medium to fine sand beaches range from dissipative to intermediate based on the morphodynamic classification of Wright and Short (1983) and are highly dynamic.

The sandy beaches are separated by a series of basaltic headlands forming closed sediment systems, named littoral cells. Up to 21 littoral cells have been identified in Oregon with lengths ranging from 10km to 100 km. The headlands extend beyond the surf zone and prevent sediment transfer from one cell to another. Therefore, each cell acts independently and the sediment budgets are

relatively stable with minor source and sinks for each littoral cell (Clemens and Komar, 1988). Minor rivers and coastal streams as well as eroding bluffs provide minimal sources to these systems while the primary sediment sinks within littoral cells are the estuaries (Allan et al., 2003). The Columbia River is a major sand source to the Pacific Northwest; however the majority of its sand is presently transported northward while minor amounts accumulate in the northernmost Oregon littoral cell (Ruggiero et al., 2005).

Each cell is highly dynamic due to the extreme forcing of the Pacific Northwest. These conditions have been studied and documented by Allan and Komar (2002). They found that annual deep-water wave heights and periods within this region are 2.2 meters and 10.4 seconds, respectively. There is a large seasonal variability between the summer and winter months. During the summer, calmer conditions persist out of the west-northwest with deep-water wave heights and periods averaging 1.2 meters and 8 seconds. In contrast, large long period deep-water waves averaging ~3 meters and ~12 seconds hailing from the west-southwest attack the Oregon coast during the winter months. It is not uncommon for deep-water wave buoys to record 7 meter waves and the extreme most waves measured in the region were over 14 meters

The tides in this region are mixed semi-diurnal with a mean range from 1-2 meters and a spring range from 2-3 meters. The tide levels also have a seasonal fluctuation with a raised winter elevation of 30 cm (Ruggiero et al., 2005). Additionally, tidal levels fluctuate over longer time scales. For example, figure 1

provided by NOAA (2007) shows the fluctuation of the average tide level at the Astoria, OR tide gauge. The combination of elevated water levels and high energy waves pose the biggest potential for coastal erosion.

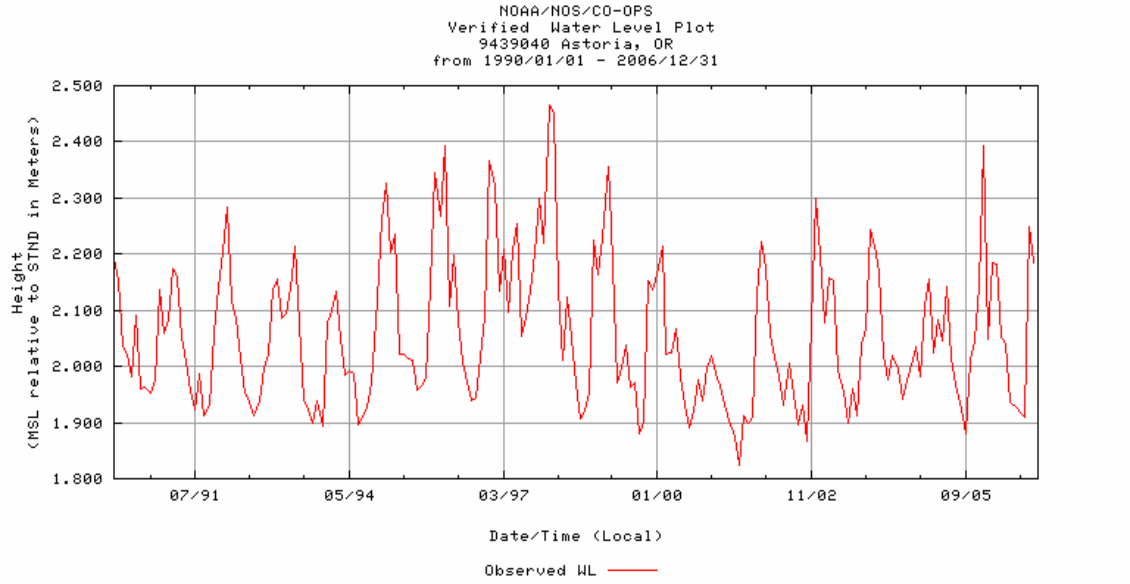

Figure 1 – Long-term tidal fluctuation

The seasonal variation of the wave forcing and water levels is complemented by a beach response. During the winter months the cross-shore beach profile flattens as sand is transported offshore to form an offshore bar. This increases the width of the surf zone allowing the large amounts of wave energy to be dissipated over a greater length. Under the calmer summer months the sand returns to the shoreline. The beach width increases as the profile steepens and often forms a summer berm.

The Oregon coastline is also affected by El Niño. These events are characterized by a warming of the waters near the equatorial Pacific Ocean; varied

sea level and storm track result. Water levels rise by tens of centimeters along the west coat of the United States during these events (Revell et al., 2002). The last major El Niño occurred during the 1997-98 winter.

Storm intensity and direction are also affected by El Niño. The subtropical jet stream is shifted south over California during El Niño bringing storms with it (Seymour, 1998). Oregon is less directly affected by storms of the El Niño as they tend to pass to the south however the waves generated from these storms still attack Oregon.

The affects of El Nino on Oregon's Netarts Littoral cell have been investigated by Revell et al. (2002). With a more acute west-southwest angle these waves are responsible for unusual amounts of longshore sediment transport to the north. This directly affects the littoral cell causing a depletion of sand in the southern region. The reduction of beach volume directly affects the beaches ability to act as a buffer between the ocean and the toes of dunes and cliffs, leaving them vulnerable to erosion episodes. The reorientation of the beach is felt long after the El Nino as it may take years for the system to recover causing a prolonged susceptibility to erosion.

2.2. Study Sites

Conditions offshore of the Oregon coastline are relatively constant however each cell acts and reacts independently of each other. The study sites selected for this study were chosen due to a known presence of rip current embayments from

published reports and anecdotal evidence. These sites are the Nehalem sub-cell, Rockaway sub-cell, Netarts sub-cell, and the Siletz sub-cell (figure 2). Each study site is a continuous stretch of beach that makes up a section of an independent littoral cell.

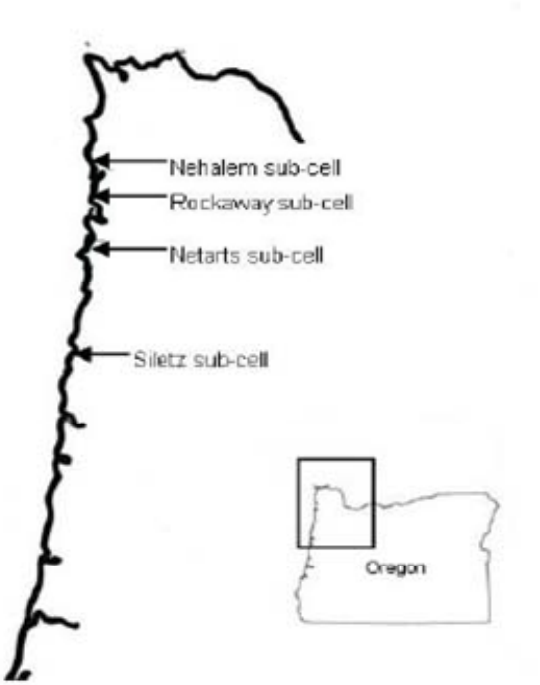

Figure 2 - Study Site Locations

These first three sub-cells, Nehalem, Rockaway, and Netarts, are characterized as dissipative beaches with fine sands O(0.2 mm). Each has an overall gentle slope and large surf zone. The Siletz sub-cell differs with its coarser medium sand grain size and a more intermediate beach profile. The affects of this difference will be discussed later.

Both the Nehalem and Rockaway sub-cells are located within the Rockaway sandy shore management cell which is bounded by Cape Falcon to the north and Cape Mears to the south. The Nehalem sub-cell is located in the northern portion of this sandy shore cell extending ~8 km from Cape Falcon to the jettied inlet of the Nehalem bay. The sub-cell contains the coastal community of Manzanita to the north while Nehalem Beach State Park is located within the southern spit. The Rockaway sub-cell is located in the center of the Rockaway sandy shore management cell. It contains ~9 km of sandy beach is bounded by two jettied inlets; Nehalem bay inlet to the north and Tillamook Bay inlet to the south. Within the Rockaway sub-cell there are three minor steams that flow through the beach. The shorelines are dune backed with an unknown amount of hardened man-made structures affecting the area.

The Netarts sub-cell is located with the Netarts sandy shore management cell and extends from the unstructured Netarts bay inlet south to Cape Lookout. This ~9 km of continuous sandy beach is mainly park land and undeveloped. Cape Lookout State Park is located in the southern end of the cell where appreciable amounts of erosion has occurred to rip current embayments (Komar et al., 1989). Backed by dunes this sub-cell is unaffected by human change and is thought to be a natural system.

The Siletz sub cell is located within the Lincoln county sandy shore management cell. A ~8km of continuous beach stretches from the natural Siletz bay inlet south to Government Point. Gleneden beach is located within this cell

where the most recent damaging embayment was observed. The beach is both dune and bluff backed. The sand is coarser here relative to the other beaches and has a steeper more intermediate beach profile.

2.3. Data for Lidar Analysis

A datum based shoreline derived from available lidar data of the Oregon coast will be used to characterize the morphological characteristics of rip current embayments. Three types of data are used in this study: lidar, wave buoy measurements, and tide gauge measurements. A summary of lidar and the lidar data used is followed below by wave and tide data information.

2.3.1. Lidar Review

Lidar is a remote sensing technique that sends out a pulse of light and analyzes the reflected transmission in order to measure distance. This technology is able to collect dense and accurate topographic data for large areas over short periods of time. A lidar system is mounted in an aircraft and is used to measure coastal topography. To extract the topographic data GPS and an internal navigation system are used to measure the aircrafts location, pitch, roll, and heading (Krabill et al., 1995). Data is collected from the airplane in an elliptical scan pattern creating a swath width approximately 50% of the aircraft altitude which is typically 700 m for beach mapping applications (Sallenger et al., 2003). To fully resolve the desired topography multiple overlapping passes are flown creating a

dense data set with a data point approximately every 2 m^2 (Stockdon et al., 2002). Each point has a root mean squared vertical error of 15 cm (Sallenger et al., 2003).

Lidar data has errors not associated with its accuracy. Lidar data may contain undesired point elevations caused by an early return signal. The first reflection of the laser is only recorded, thus both land and water surface elevations are recorded and must be separated (Revell et al., 2002; Stockdon et al., 2002). Occasionally birds, tall vegetation and clouds can cause a return. Since clouds can cause interference lidar flights are often flown during periods of fair weather.

Applications of lidar data related to coastal engineering are typically focused on shoreline change and dune erosion. The use of lidar data has proved very useful in previous research to quantify beach change (Revell et al., 2002). Lidar in the present application will be used to establish a shoreline contour. The variability of this contour is then analyzed.

2.3.2. Lidar Study Data

The lidar data used in this study were collected on October 17, 1997, April 28, 1998 and September 20, 2002. The processed lidar data is made available on the NOAA website and using the LIDAR data retrieval tool individual areas encompassing the study sites for each date was downloaded (NOAA 2007a). The data were projected into the 1983 Oregon State Plane North zone using NAVD88 as the vertical datum. Both projection units and vertical units are in meters. The

outputted x, y, z data was processed and put into a 5 meter grid relative to northings and eastings.

Data used in this study only includes sandy shores within the sub-cells. The boundaries, headlands and inlets, are not included because they interfere with the location and analysis of the shoreline contour. To remove this interference the limits of each sub-cell data was collected at a distance from each boundary. Limits placed on the northings (Oregon state-plane north) of the lidar surveys for each sub cell are shown in table 1.

Table 1 - Lidar collection limits

Sub-cell	South Limit [m]	North Limit [m]
Nehalem	227300	235100
Netarts	193400	202000
Rockaway	218000	226650
Siletz	138000	145500

2.4. Tide and Waves

Lidar returns from the water surface do not represent topographic data; and hence, these returns are treated as noise and removed. In order to define water surface returns local water levels are estimated using tide and wave data.

There is little tidal variation along the Oregon coastline. A single tide gauge is used to determine the tidal elevation at each study site for the survey periods. Using data collected by NOAA at the Astoria, OR tide gauge (Station ID:

9439040) tidal elevations relative to NAVD88 at six minute intervals were downloaded from the NOAA tides and current website (NOAA 2007b).

The local water surface elevation induced by waves is the wave runup. Estimates of runup amplitudes can be calculated using empirical formulas (discussed in a later section). The common inputs for these calculations are the wave characteristics present during the study period. Measurements of hourly wave height and period are collected by NOAA's National Data Buoy Center and are downloaded from their website (NOAA 2007c). The hourly wave height recorded is the significant wave height calculated as the average of the highest one-third of all of the wave heights during a 20 minute sampling period. The dominant wave period is the period with maximum wave energy.

Wave conditions during the survey period data were downloaded from the Stonewall Banks buoy, station 46050. This is a 3-meter discus buoy located 20 nautical miles West of Newport, OR at a water depth of 130 m. Although this buoy is located south of the study sites it is believed that waves recorded at this station are comparable to the conditions offshore of the study sites. The average conditions during the survey dates are shown in table 2. Wave conditions during the survey dates are relatively equal and mild for the Pacific Northwest.

Table 2- Average wave conditions during lidar surveys

Date	Dominant Wave Height [m]	Dominant Wave Period [sec]
17-Oct-97	1.67	10.5
28-Apr-98	1.42	10.85
20-Sep-02	2.32	10.32

Also of interest are the wave conditions prior to the survey period. The antecedent wave conditions may provide a clue of the life cycle of embayments and the conditions necessary for embayments to generate and persist. Due to a lack of data prior to the survey periods a separate buoy is used to collect the antecedent wave conditions. NDBC station 46002 located 275 nautical miles West of Coos Bay, OR provided the most complete set of antecedent wave conditions. This station consists of a 6-meter NOMAD buoy that is stationed at a water depth of 3,374 meters.

3. Methodology

A method for the identification and measurement of rip current embayments is now presented. Based on the lidar data, a datum based shoreline is established. This shoreline is then filtered to isolate shoreline variations that represent embayments. The embayment features are then identified and measured.

3.1. Datum Based Shoreline

To consistently analyze shoreline variability through a beach history a constant definition of the shoreline is needed which has minimal variation in space and time (Boak and Turner, 2005). Shoreline indicators such as morphological features or water levels are subjective and have limited repeatability whereas tidal-based shorelines are objective.

A tidal-based shoreline is derived from the intersection of the beach profile with a local tidal datum. Although the calculation of each tidal datum is defined, there is a world wide tidal fluctuation so these values are relatively site specific. For example, mean high water (MHW), the average measure of all high water levels during a 19 year tidal epoch, in Astoria, OR is 2.1 m NAVD88 while in Atlantic City, NJ it is 0.5 m NAVD88. A tidal based shoreline is relative to each location and comparisons of the shoreline between separate regions can be made using tidal datums.

To use a tidal datum to establish shoreline position it is necessary to be able to survey at the specified elevation. Water level is the basis for tidal datums;

therefore at any given point in time a tidal datum may be inundated or exposed. At these levels on the beach face morphologic change can occur on the order of tidal cycles. Where as traditional surveys could not collect large dense surveys at this time scale lidar data can with the use of aircraft. Most lidar flights are collected during periods of lowest tide to collect as much sub-aerial beach as possible.

The selection of the vertical tidal datum defining the shoreline has a direct influence on the measurement of the morphological features of rip embayments. Varying in both the cross-shore and longshore direction rip embayments are three dimensional features that exist from an unknown depth offshore to the beachface.

Providing guidance to the selection of the tidal datum is a survey of a recent rip current embayment (figure 3). This land based survey of a rip current embayment was collected at Rockaway Beach, OR in May 2005 by Jonathan Allan of DOGAMI (Allan 2006). This feature remained through the summer months but was undetectable in October 2005. Data was collected using a Trimble 5700/5800 RTK-DGPS surveying system mounted on an ATV. The survey ranged from mid-beach to an unknown depth within the surf zone encompassing elevations from 0 to 5 meters NAVD88. The sub-aqueous data provided a more detailed description of an embayment that is not visible to lidar surveys.

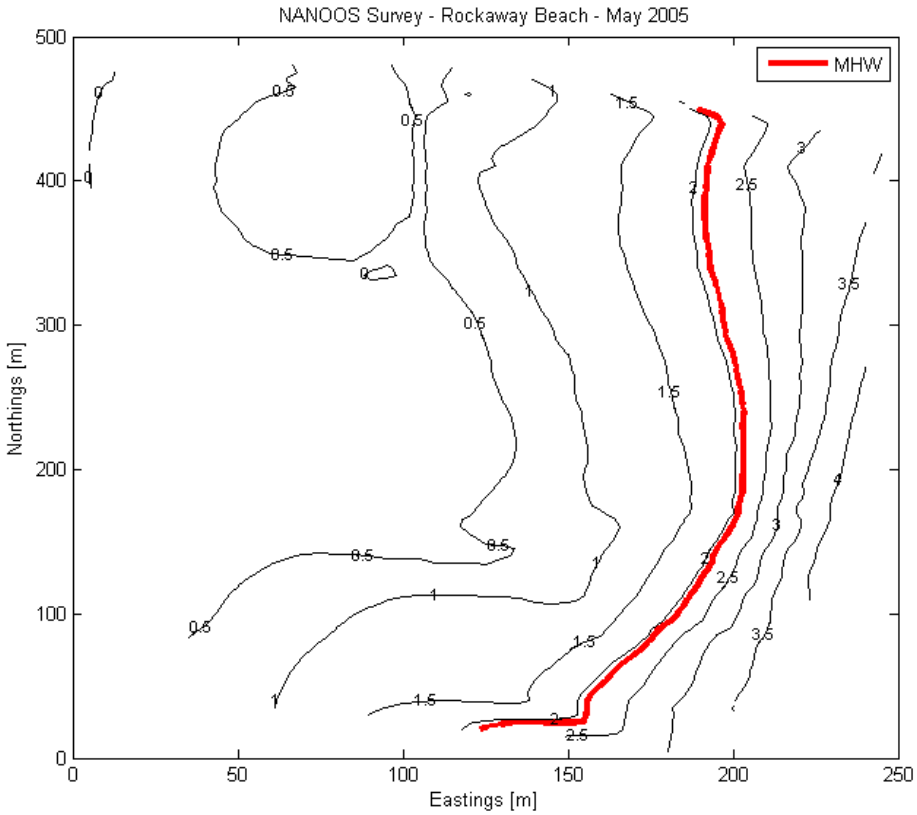

Figure 3 – Land based survey of an embayment

The variability in the shoreline contours associated with this feature decrease with elevation. However, the longshore extent of the feature is relatively unchanged for a range of contour elevations. These relationships are seen in figure 3 where the MHW shoreline is indicated by the bold line. This elevation contour can also be surveyed at low tide by land based methods such as those used by Jonathan Allan.

The location of the embayment in figure 3 is within the Rockaway sub-cell of this study. This survey provides insight into the selection of the datum to

represent the shoreline. The embayment is more defined at lower elevations; however, the lower elevations are not accessible through lidar data. The desired datum is one that has an elevation close to the water level while being accessible to lidar surveys.

The mean high water tidal datum is chosen to define the shoreline in this study. The mean high water elevation is the average of all high tides of a 19 year epoch period. In Oregon, there is little tidal variation along the coastline resulting in a constant value of MHW equal to 2.1 meters NAVD88 (Weber et al 2005). For all study sites this constant value is used.

3.2. Establishing Shoreline Contours

A shoreline contour is calculated from the lidar data collected from the NOAA website. The lidar data is in a 5 meter grid data set. This provides eastings cross-shore transects every 5 meters along the beach. The beaches of the study site have a minimal angle from true north and thus these eastings profiles are taken to be representative of cross shore profiles. From each cross shore profile the intersection of the beach face and MHW elevation of 2.1 meters NAVD88 is computed. Contours ranging from 1 meter to 5 meters with a 0.5 meter interval are also calculated if they can be resolved form the data.

Extraction of shorelines from lidar data is highly dependent upon noise within the data caused by water surface elevations in this study. Stockdon et al. (2002) were able to remove noisy water returns from lidar cross-shore profiles

using the tidal elevations and wave run-up during the survey period. Average wave conditions and the resulting run-up are shown in table 3. Run-up calculations we made using an empirical formula derived by Holman (1986).

$$R_{2\%} = H_o\left(0.83\xi_o + 0.20\right), \text{ where}$$

$$\xi_o = \beta \Big/ \sqrt{H_o / L_o}$$

β is the foreshore beach slope and taken as 0.03, and H_o and L_o are the offshore wave height and length. This equation for $R_{2\%}$ calculates the 2% exceedence levels of run-up and is a conservative number.

Table 3 - Wave conditions and run-up values

Date	H_s [m]	T_s [sec]	$R_{2\%}$ [m]
17-Oct-97	1.67	10.5	0.76
28-Apr-98	1.42	10.85	0.69
20-Sep-02	2.32	10.32	0.95

The combined tide levels plus average run-up for the dates our lidar data was collected is shown in figure 4. Multiple lidar surveys were flown on October 17, 1997 and September 20, 2002 due to weather conditions. Data collected during these dates were likely combined during post processing. The mid-tide and low-tide from 1997 and 1998 shown in figure 4 are consistent with those documented by Revell et al. (2002). Due to the uncertainty of the flight time, we were unable to develop a definitive cut-off elevation and a separate method is used to establish beach contours.

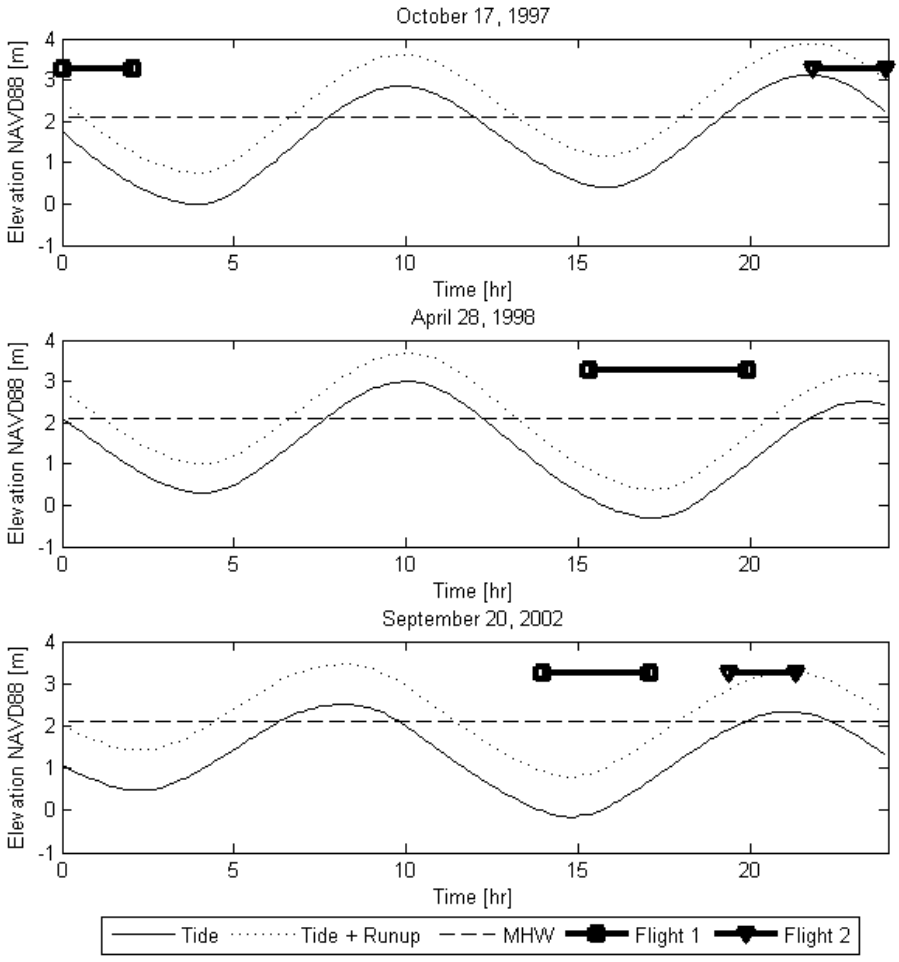

Figure 4 – Estimated water levels during lidar flights.

Lidar data collects more than the desired beach face elevations. Seaward of the beach; water surface elevations are collected. Landward of the beach; dune, cliff, and bay system elevations are collected. Removal of this extra data reduces computation time and increases the accuracy of the results. Excess data is removed by calculating a base shoreline contour and excluding data outside of a buffer limit.

The base shoreline is calculated at an elevation of 3.5 meters. This elevation was chosen because it is above the MHW tidal datum but is believed to be below an average dune toe elevation. Locations of this contour are calculated from five cross-shore transects every 500 meters. The cross-shore transects are averaged and the intersection of this average profile and a 3.5 meter elevation represent the location of the base contour.

This base contour is used to eliminate excess data that has a distance greater than 250 meters landward and seaward from the contour. The base shoreline at a 500 meters spacing interval is interpolated to five meter spacing interval so that each profile can be buffered. Once each profile has been buffered and excess data removed the location of shoreline contours is calculated.

The location of the intersection of the beach profile and desired shoreline contour elevation is found using only the buffered data points. The number of points is further reduced along each profile. Points located seaward and landward of the minimum and maximum profile elevations are removed. The remaining points are used to locate the beach contours. Locations of the intersection point between the beach profile and the desired elevation is made by finding the most seaward point greater than the desired elevation and the most landward point less than the contour elevations. If these points are not located less than 5 points or 25 meters away the location of the desired contour elevation at the beach profile is not found. This error is a result of noise from water surface returns. This process is shown in figure 5. In the top panel data points the circles identify points selected

form the maximum and minimum of the buffered points. The bottom panel shows the linear interpolation to the MHW elevation.

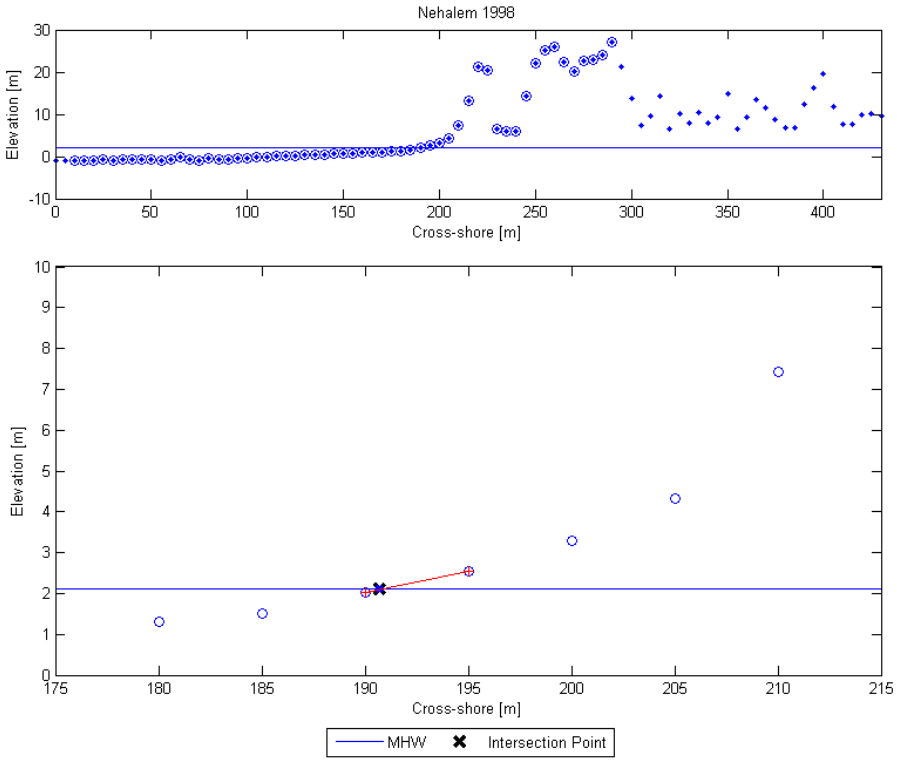

Figure 5- Identification of the MHW contour

The percentage of verified data points is collected for each beach and survey period. 95% completeness is required for the MHW shoreline to pass to analysis. Elevated water levels during the 1997 survey provided only 75% of the MHW contour at the Nehalem sub-cell and 83% of the MHW contour at the Rockaway sub-cell. The 1997 survey of the Siletz data only provides 41% of the MHW contour because the lidar survey passed landward of the beach. At all other times and locations 99% of the MHW contours was found.

The slope of the MHW contour is also calculated. For each cross-shore transect the slope is calculated by placing a linear regression through the points 0.5 meters above and below the MHW elevation. The slopes of these points represent the foreshore beach slope.

3.3. Band-pass Filter Shoreline

It is not necessarily straightforward to identify embayments in the raw irregular shoreline contour. Irregular shorelines typically contain multiple morphologic features with a range of length scales at any given time. To identify rip current embayments we first specify a range of expected length scales. Using this range of scales we apply a bandpass filtering operation to the shoreline contour to identify potential rip current embayments.

It is expected that rip embayments are separate and larger than beach cusps. Beach cusps can range from 1 to 100 meters (Blondeaux 2001) thus 100 meters sets the lower limit length scale of embayments. At large scales the embayments must be separated from the overall relative shoreline curvature. In previous studies of large scale shoreline response (Allan et al 2003 and List et al 2005) cutoff limits of 1000 and 1500 meters were used to identify the overall shoreline response. Still present in the 1000 meter limit were very large rip current embayments; however rip embayments were not observed when using the 1500 meter limit. Therefore to include these large rip embayments while eliminating the large-scale shoreline response an upper limit of 1500 meters is set.

To reveal the desired embayments a filtering process is applied that results in an effective bandpass between the 100 and 1500 meter scales. The filtering process consists of two separate filters that are then coupled to create the bandpass shoreline. The original MHW contour is first filtered using a 100 meter window, effectively removing all features having a length scale less than 100 meters. This filtered shoreline will be referred to as MHWbp1. As mentioned before this eliminated the presence of beach cusps but it also eliminated the high frequency noise of the contour line. This noise is thought to be caused by the ~15cm vertical error inherent in lidar surveys (Sallenger et al., 2003). This vertical error can create a horizontal error of 6 meters on a beach with a 1:40 slope. Next the origional MHW contour is filtered using a 1500 meter window removing all features having a length scale less than 1500 meters and this represents the overall shoreline curvature. This filtered shoreline will be referred to as MHWbp2. By subtracting the 1500 meter filtered MHW contour from the 100 meter filtered MHW contour the original shoreline has been bandpassed at 100-1500 meters (MHWbp2-MHWbp1=MHWbp) leaving features with these length scales less than 1500 meters but greater than 100 meters.

This process is shown in figure 6. Positive values of the MHWbp shoreline represent areas where the local shoreline is landward of the base shoreline while negative values represent areas where the local shoreline is seaward of the base shoreline.

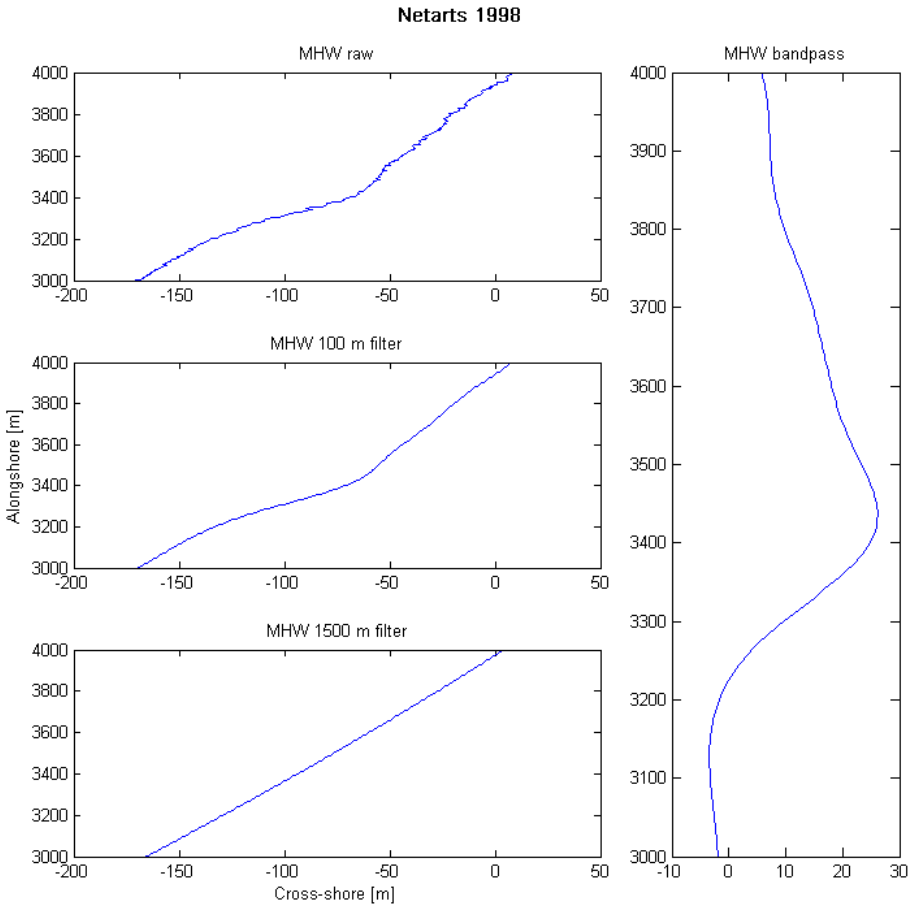

Figure 6- Bandpass filtering process

The filter function used to process the shoreline is the 'filtfilt' function in MATLAB. This function has zero phase distortion because the input data is filtered both in the forward and reverse direction using a user specified filter window of 100 and 1500 meters. This function also matches the endpoints of the original shoreline to minimize start-up and ending transients. This reduced the ability of embayments to appear at the endpoints of the shoreline. The endpoints of the shoreline are bounded by either a natural inlet or a shore-normal structure.

At natural inlets embayments are not expected to form. The shore-normal structures, such as a basaltic headlands or jetties, often create rip currents and can generate embayments. This study is focusing on embayments that form on open coasts.

3.4. Embayment Identification

Next, Individual embayments are extracted from the MHWbp shoreline and their morphologic characteristics are measured. Three critical points must be identified to extract the embayment; the embayment, north horn, and south horn. These points are shown in figure 7.

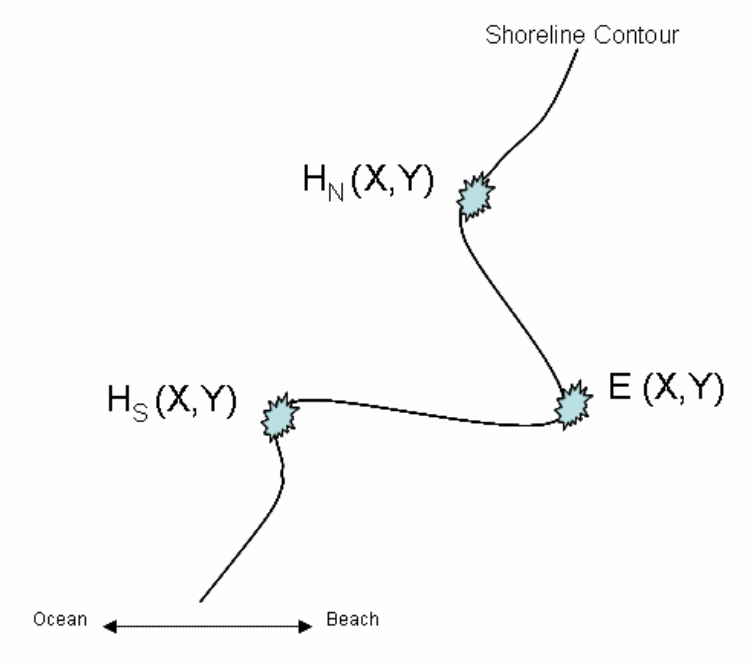

Figure 7 - Critical embayment points

Identification of the critical points for each embayment along the shoreline is made using a multiple minimum and maximum method (Kopentko, 2003). This

method identifies local points of maximum and minimum values of the bandpass shoreline. Variability of the bandpass shoreline represents local regions (<1500 meters) of erosion or accretion relative to the overall shoreline. Local maximum shoreline points correspond with embayments while minimum shoreline points correspond with horns.

The extraction of embayments is a two part process. First the location of the horns is identified. Then the embayment points between the horns are identified. Each embayment must have two horns to be identified. Areas adjacent to the endpoints are not considered embayments until a horn is first present, thus erosive areas adjacent to the endpoints are overlooked. The endpoints are located adjacent to headlands and inlets, therefore the erosion at these locations is separate from erosion caused by rip current embayments and are not considered in this study.

The ability to accurately identify the embayment features is dependant on a sensitivity of the multiple maximum and minimum methods. The sensitivity determines how defined a local maximum must be to be identified. The setting has a range of 0 (highly sensitive) to 10 (low sensitivity). Using a low sensitivity setting the location of isolated embayment horns will drift further along the adjacent beach increasing the length of embayments. Under high sensitivity all local maximum, such as small scale features on a relatively straight section of beach left by the filtering process are identified. Calibration was necessary to identify only critical points of plausible embayments. Comparisons between

manually and computer identified points at all locations were preformed. Sensitivity values were steadily increased from zero using integer values. A value of 4 provided the optimal locations for the horns and embayments while also identifying sections of beach unaffected by embayments. These unaffected sections of beach are removed using threshold criterion described in the next section.

3.5. Embayments Measurements

3.5.1. Individual

Our extraction method provides the locations of the three critical points of each embayment on the bandpassed shoreline. For more accurate measurements, the locations of the critical points are translated from the filtered shoreline to the 100 meter lowpass filter. Large scale features are present within this shoreline providing more accuracy. Each plausible rip current embayment is measured using the three critical points; north horn, embayment, and south horn. The measured morphological characteristics include: length, amplitude, aspect ratio, skewness (figure 8).

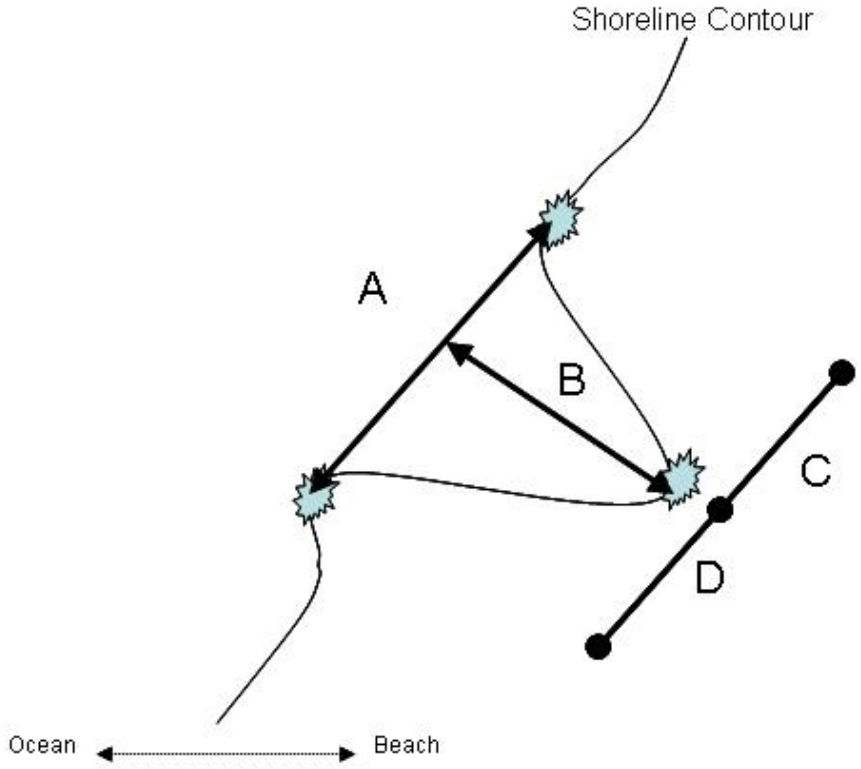

Figure 8 – Embayment morphological characteristics

The length of the embayment represents the longshore extent of the embayment on the datum-based shoreline. This length is calculated using the locations of the north horn $H_N(x,y)$ and the south horn $H_S(x,y)$ on the shoreline. The length of the shoreline is the straight distance calculated using Pythagoreans Theorem from the north and south horns. The equation of the line in the form $Ax+By+C=0$ representing the length was calculated at this point and is used in the amplitude calculation.

The amplitude of the embayment represents the cross-shore extent of the embayment on the datum based shoreline. The magnitude of the amplitude was calculated as the shortest distance from the embayment point, E(x,y) to the length line equation Ax+By+C=0. The shortest distance being a perpendicular distance is calculated using

$$Amplitude = \frac{A * E(x) + B * E(y) + C}{\sqrt{A^2 + B^2}}$$

The amplitude line has a slope equal to the negative inverse of the length line. Using the slope of the length line and the amplitude distance, the intersection point I(x,y) is identified to be used in later calculations.

The maximum erosion point for embayments is not often located equidistant from the horn or on the center of the embayment. The skewness of the embayment is used to measure the symmetry of the embayment. Skewness is calculated by subtracting the distance of the North horn to the intersection point by the distance of the South horn to the intersection point and dividing by the total length. These distances are calculated using the locations of the north horn $H_N(x,y)$, south horn $H_S(x,y)$, and intersection point I(x,y) on the shoreline. A value of zero indicates a symmetric embayment with the point of maximum erosion located equidistant from the horns. Values less than and greater than zero indicate the maximum point of erosion is located nearer the south and north horn respectively.

The last morphological characteristic calculated for each embayment is the aspect ratio of the embayment. The aspect ratio indicates the shape of the embayment with a relationship between the length and amplitude of each embayment. By dividing the embayment width by the embayment length the aspect ratio is calculated. Larger values of this ratio represent less erosive embayments per width.

As a final quality control for embayment identification, each embayment must meet a length and amplitude threshold criterion. A minimum length of 100 meters is required for any identified shoreline undulation to be considered a plausible embayment. This threshold eliminates a small scale feature (or high frequency noise) that was not removed through filtering process. Minimum amplitude of 5 meters is required for a shoreline undulation to be considered an embayment. This threshold eliminated relatively straight sections of shoreline between two successive horns that separate isolated embayments.

3.5.2. Spatial Relationship

Not only are the individual morphological characteristics of embayments important but so are their spatial relationships for each study site. If such a relationship is found, how might it be affected with time? In an attempt to unearth these relationships additional calculations were made.

The number of embayments per survey period at each study site is collected. To provide a comparison between the separate sub-cells the number of

embayments is divided by the study site length to provide a number of embayments per kilometer of study site. Also relative to the number of embayments per beach, the percentage of beach affected by the embayments is calculated by dividing the total length of the embayments by the total length of the study site.

The relative location of each embayment in the sub-cell is recorded. Values of the relative location range form 0 – 1, representing the south and north limit of the sub-cell, respectively. This measurement is used to identify preferential location of embayments. The mean of these values are calculated for each beach to provide and general preference per study site per date. A value of 0.5 would represent the embayments are centered on the center of the study site. Values less than and greater than 0.5 indicate an overall preferred location to the south and north, respectively, to the center of the study site.

The mean and standard deviation of the embayment spacings are calculated for a given study site and survey period. The spacing is calculated as the distance from successive embayment points. This calculation does not consider the distance between the horns of two successive embayments. The standard deviation of the spacing will provide insight as to the rhythmic nature of embayments.

The mean, standard deviation, and kurtosis for each individual morphological characteristic for each study site and survey are calculated. The kurtosis describes the distribution of the data. Negative values indicate a relatively

flat distribution. Positive numbers indicate a peaked distribution. A value of zero indicates a normal distribution.

3.6. Summary

The location of the MHW elevation is identified for each profile spaced at 5 meters in the alongshore. These points create the datum based MHW shoreline. Through a bandpass filtering process, shoreline variability with length scales between 100 and 1500 meters are extracted. Local points of maximum shoreline variability are identified using a multiple minimum and maximum method. Plausible embayments, consisting of an erosive embayment point and two horns, are identified and measured. Individual embayment measurements consisting of the length, amplitude, skewness, and aspect ratio are conducted. An embayment must meet a threshold of having length and amplitude greater than 100 and 5 meters respectively. Relationships between the individual embayments along a study site through time are sought out.

4. Lidar Embayment Results

Using the described method plausible rip current embayments are extracted from a filtered MHW shoreline. A total of 98 embayments were extracted and measured from a total of ~75km of total surveyed beach. On average ~11 embayments were identified at each study site for each survey period. The total length of the embayments is ~58 km, thus embayments occupy ~77% of the study sites. A summary of the results is first presented, followed by an analysis of individual study site locations. A complete list of the results is found in the appendix.

4.1. Summary of all Embayments

A total of 98 embayments were identified from 9 sets of data; two lidar surveys, 1998 and 2002, at each of the four sub-cells and the1997 survey for the Netarts sub-cell. These embayments are all unique with varying characteristics and location.

Embayments occupy a major portion of the beach for each study cell. The total length of embayments present at a given survey date per location is divided by the corresponding beach length. The results shown in table 4 indicate that embayments occupied anywhere between 58 and 93% of a sub-cell, with an average occupation of 77%.

Table 4 - Percentage of beach occupied by an embayment

Location	Year	Beach Length [m]	Total Embayment Length [m]	% Beach occupied by embayments
Nehamlem	1998	7800	5679	73
	2002		7154	92
Rockaway	1998	8770	7023	80
	2002		7600	87
Netarts	1997	8710	5860	67
	1998		7061	81
	2002		5897	68
Siletz	1998	7730	7172	93
	2002		4448	58
Total	**-**	**74730**	**57894**	**77**

The morphological characteristics of individual embayments of length, amplitude, aspect ratio, and skewness, were calculated and analyzed. The range, average, standard deviation, and kurtosis for all the embayments are shown in table 5. On average the measured embayments at our study sites have a length and amplitude of 591 and 18 meters, respectively. These length scales have a large standard deviation relative to the average describing the variability of sizes of embayments. The length of the embayments has a near normal distribution while the distribution of the amplitude is more peaked and skewed towards the smaller amplitudes.

Table 5 - Morphological characteristics of all 98 measured embayments

	Length [m]	Amplitude [m]	Aspect Ratio -	Skewness -
Range	266 - 1256	5 - 59	14.2 - 142.1	-0.73 - 0.64
Mean	591	18	42.3	-0.1
Standard deviation	219	12	23.8	0.3
Kurtosis	0.6	2.3	3.0	-0.6

The relationship between the length and amplitude of each embayment is shown in figure 9. Two traits are seen in the figure; a general linear trend and a clustering effect. A linear regression is fit to the data giving a function for the length of the embayment in terms of amplitude. The degree to which the linear regression represents the data is shown with the R^2 value of 0.4. However, barring three embayments, with a large length and small amplitude, the data appears to follow this trend line. There is a higher concentration of embayments having lengths, 250-850 meters, and corresponding amplitudes, 5-30 meters. Multiple embayments are located adjacent to the 5 meter amplitude threshold where a few are located near the 200 meter length threshold, thus the amplitude threshold has greater weight.

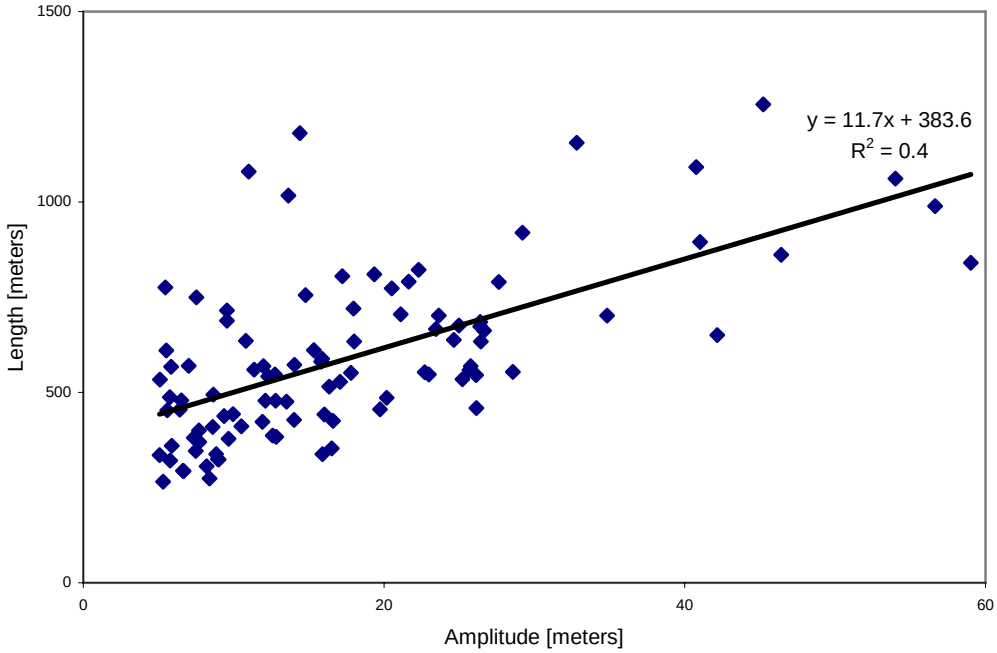

Figure 9 – Length/amplitude relation of all measured embayments

Secondary features calculated are the aspect ratio and skewness. The average aspect ratio is 43; on average an embayment will have a length 43 times the amplitude. This does not represent a growth pattern but rather the scalar relationship at one point in time. The average skewness is -0.1; thus the maximum point of erosion is slightly located towards the south horn.

The mean of the relative location of the most erosive point of the embayments is 0.5. This value as well as the negative kurtosis value and the range of the relative location indicate the embayments were distributed across the study sites and not concentrated in a specific region. This is also seen in the mean and standard deviation of the embayment spacing.

4.2. Study Site Results

Each study site is a part of a larger littoral cell. The Nehalem and Rockaway sub-cell are both located within a single littoral cell. The Netarts and Siletz sub-cells reside in two separate littoral cells. With an assumed equal offshore wave forcing these littoral cells have a beach response independent of each other and each study site is considered separately to determine if each sub-cell has a distinct embayment signal.

4.2.1. Nehalem Sub-cell

A total of 22 embayments were extracted from the 7.8 km dissipative Nehalem sub-cell beach using the 1998 and 2002 Lidar data. A summary of the measurements is shown in table 6. The ten 1997 embayments and 12 1998

embayments have an average length and amplitude of 583 meters and 20 meters, respectively, near the overall average. A linear relationship between the length and amplitude is shown in figure 10. The relative embayment location is slightly south of center with the embayments having a skewness value near symmetry and an average aspect ratio of 34.

Table 6 - Nehalem sub-cell measurements

Measurement			1998	2002	Average
Beach Length		**[km]**	7.8	7.8	**7.8**
Embayment Count		**#**	10	12	**11**
Embayments/km		**[1/km]**	1.28	1.54	**1.42**
Mean Location		**-**	0.40	0.48	**0.45**
Spacing	**Average**	**[m]**	**666**	**650**	**657**
	Standard dev.	[m]	336	291	
Length	**Average**	**[m]**	**568**	**596**	**583**
	Standard dev.	[m]	124	284	
	Kurtosis		-1.05	1.26	
Amplitude	**Average**	**[m]**	**18**	**22**	**20**
	Standard dev.	[m]	8	13	
	Kurtosis		-1.87	0.58	
Aspect Ratio	**Average**	**[m]**	**36**	**32**	**34**
	Standard dev.	[m]	11	12	
	Kurtosis		-1.64	-1.37	
Skewness	**Average**	**[m]**	**-0.04**	**-0.12**	**-0.08**
	Standard dev.	[m]	0.22	0.26	
	Kurtosis		-1.38	-1.19	

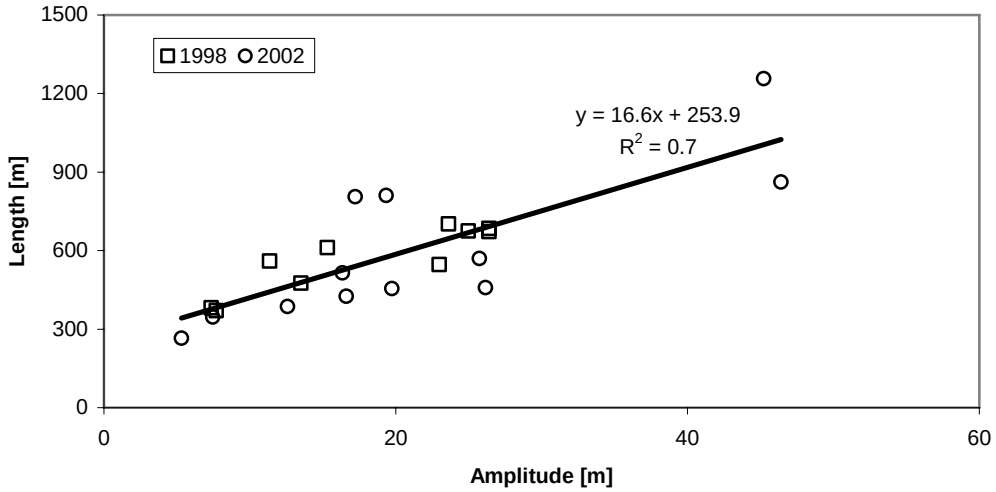

Figure 10 - Nehalem sub-cell length/amplitude relation

Comparisons between the separate survey periods were made. The embayments from the 2002 survey period have increased in length and amplitude 5% and 20% respectively. This is also shown in the decrease in the aspect ratio, thus the embayments have relatively same length scale though the amplitude has increased. The skewness of the embayments changed from near symmetry to slightly skew to the south. There is no obvious correlation between the relative locations of individual embayments for the separate survey periods (figure 11) to indicate preferential location. The mean location of the embayments, represented by the vertical line in figure 11, indicates the embayments are located south of the study site center both years.

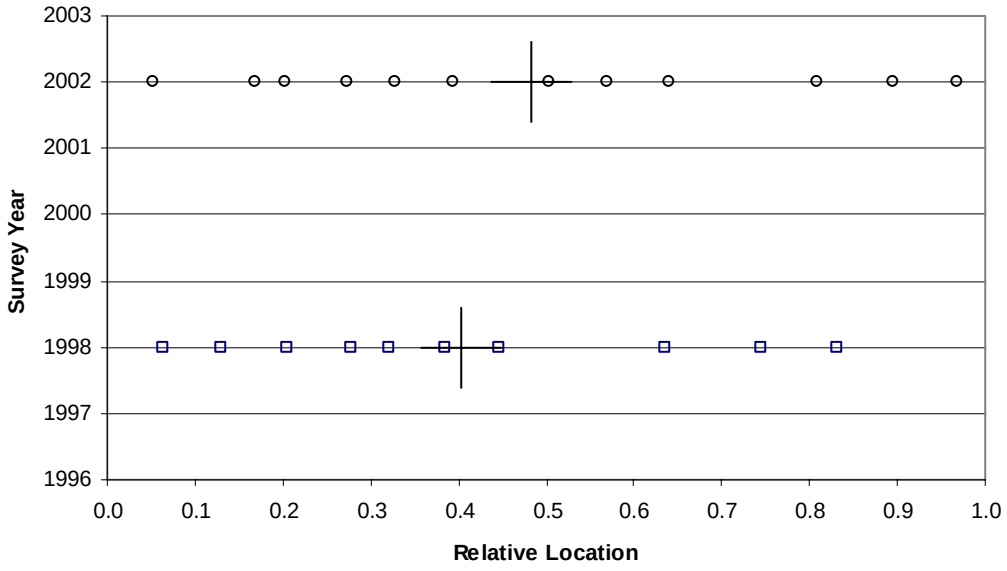

Figure 11 - Nehalem sub-cell embayment location

4.2.2. Rockaway Sub-cell

A total of 23 embayments were identified along the 8.8km of the dissipative Rockaway sub-cell using the 1998 and 2002 lidar survey data. A summary of the measurements from this sub-cell are show in table 7. The average embayment length and amplitude within this sub-cell are 643 and 21 meters, respectively. Both values are larger than the overall averages. The linear relationship between the length and amplitude at this location is shown in figure 12. The average relative embayment location is at the center of the study site with the embayments having a slight skew towards the north with an aspect ratio of 41.

Table 7 - Rockaway sub-cell measurements

Measurement			1998	2002	Average
Beach Length		**[km]**	8.77	8.77	8.77
Embayment Count		**#**	12	11	11.5
Embayments/km		**[1/km]**	1.39	1.27	1.32
Mean Location		**-**	0.52	0.48	0.50
Spacing	**Average**	**[m]**	**677**	**717**	**699**
	Standard dev.	[m]	324	317	
Length	**Average**	**[m]**	**585**	**691**	**643**
	Standard dev.	[m]	245	260	
	Kurtosis	**-**	1.36	-0.34	
Amplitude	**Average**	**[m]**	**18**	**24**	**21**
	Standard dev.	[m]	15	16	
	Kurtosis	**-**	1.91	0.64	
Aspect Ratio	**Average**	**-**	**46**	**37**	**41**
	Standard dev.	**-**	26	17	
	Kurtosis	**-**	2.49	0.99	
Skewness	**Average**	**-**	**0.05**	**-0.20**	**-0.07**
	Standard dev.	**-**	0.35	0.36	
	Kurtosis	**-**	1.37	-1.03	

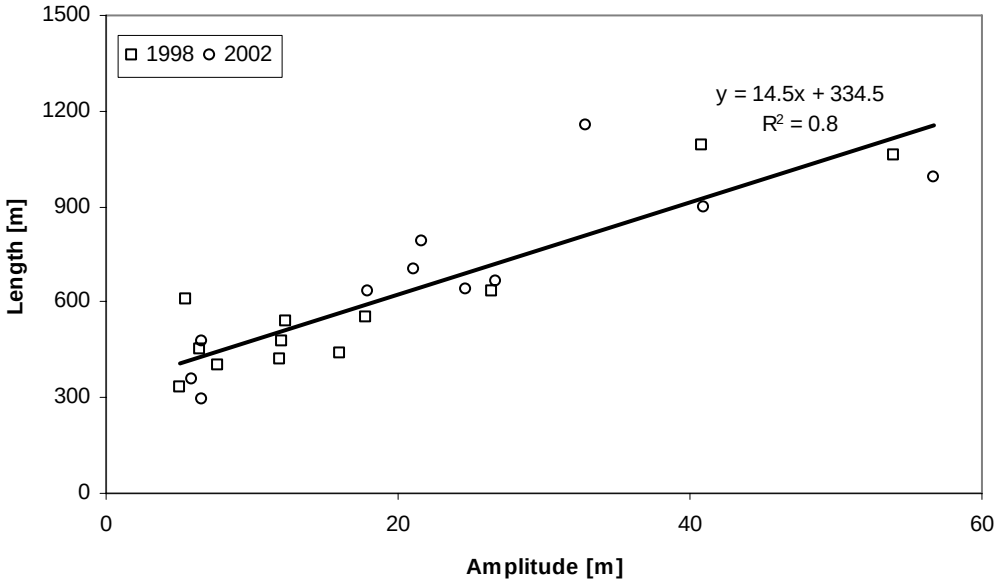

Figure 12 - Rockaway sub-cell length/amplitude relation

Comparisons between the study periods were made. The length and amplitude of the embayments from the 2002 survey have increased 18% and 32%, respectively, which is mirrored with the decrease in the aspect ratio. The relative location of the embayments shifted to the south. Also the skewness of the embayments reoriented from north to south. There is no obvious correlation between the relative locations of individual embayments for the two survey periods (figure 13) to indicate a preferential location. The mean location of the embayments (vertical line in figure 13) is located near the center for both years.

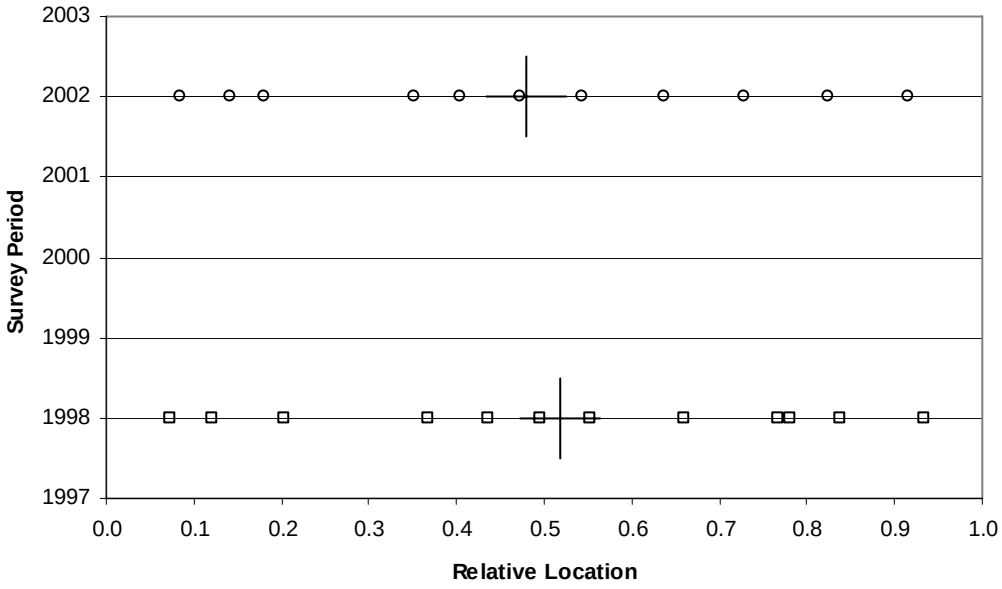

Figure 13 -Rockaway sub-cell embayment location

4.2.3. Netarts Sub-cell

A total of 30 embayments were identified along the 8.7km of the dissipative Netarts sub-cell from the 1997, 1998, and 2002 lidar survey data. A summary of these measurements are shown in table 8. Ten embayments are present within each survey period of this sub-cell with an average length of 627 meters, greater than the overall average, and amplitude of 13 meters, less than the overall average. The linear relationship between the length and amplitude of this sub-cell are shown in figure 14. The average relative embayment location is located slightly south of the study site center. On average the embayments are skewed to the north with an aspect ratio of 59. Although the number of embayments for each survey is equal their characteristics are different.

Table 8 - Netarts sub-cell measurements

Measurement			1997	1998	2002	Average
Beach Length		**[km]**	8.71	8.71	8.71	8.71
Embayment Count		**#**	10	10	10	10
Embayments/km		**[1/km]**	1.16	1.16	1.16	1.16
Mean Location		**-**	0.46	0.60	0.38	0.48
Spacing	**Average**	**[m]**	**720**	**815**	**737**	**757**
	Standard dev.	[m]	357	434	368	
Length	**Average**	**[m]**	**586**	**706**	**590**	**627**
	Standard dev.	[m]	122	280	206	
	Kurtosis	**-**	-0.85	-0.69	0.79	
Amplitude	**Average**	**[m]**	**9**	**14**	**15**	**13**
	Standard dev.	[m]	5	6	7	
	Kurtosis	**-**	4.38	3.95	0.36	
Aspect Ratio	**Average**	**-**	**77**	**53**	**47**	**59**
	Standard dev.	**-**	32	24	25	
	Kurtosis	**-**	0.47	-0.54	1.12	
Skewness	**Average**	**-**	**0.00**	**0.04**	**-0.11**	**-0.02**
	Standard dev.	**-**	0.34	0.39	0.22	
	Kurtosis	**-**	0.76	-1.46	-0.43	

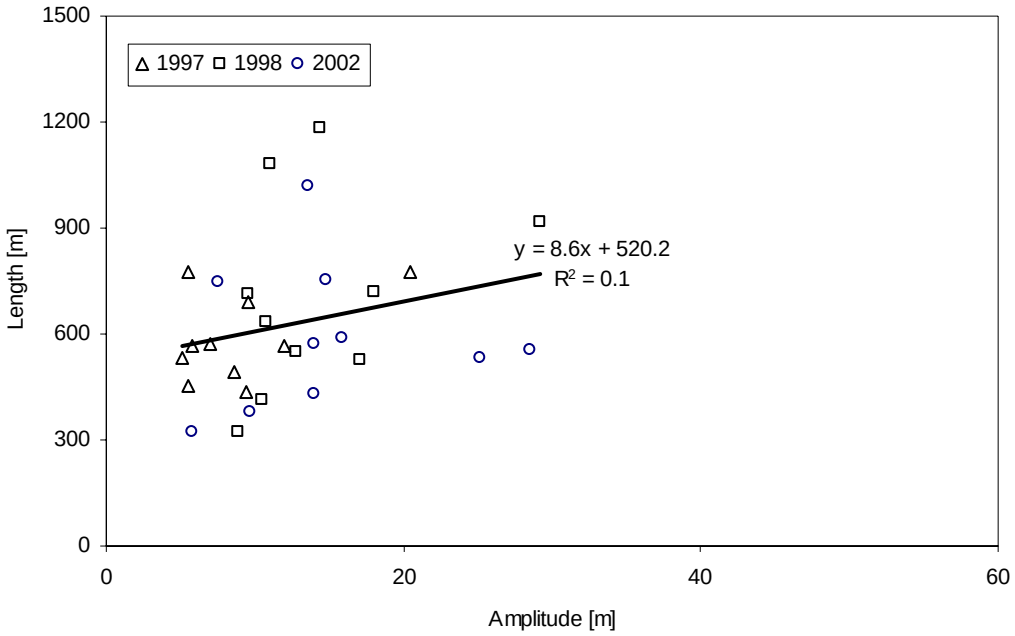

Figure 14 - Netarts sub-cell length/amplitude relation

The Netarts sub-cell is special because the shoreline was resolved from the 1997 lidar survey. The effects of an El Niño winter can be seen by comparing the 1997 and 1998 lidar surveys that were taken 7 months apart. The average length and amplitude calculated during the 1998 survey period is 706 and 14 meters respectively. This represents a 21% increase in length and a more noticeable 60% increase in amplitude over the previous survey. This change is mirrored in the reduction of the aspect ratio by 30%. The relative location of the embayments is shifted to the north by 1.2 km. The mean location of the embayments shifted further north during this event sown in figure 15 (vertical lines represent mean embayment location).

Comparisons between the 1998 and 2002 survey data were made. There is a 17% reduction in embayment length for the 2002 embayments. The amplitude, however, is 5% greater. For this survey period the embayments have the smallest aspect ratio when compared to the other survey period within this study site. The relative location of the embayments is located 1.9km south of the previous survey. The maximum point of erosion is located in the southern portion of the embayment in 2002 where as it was in the north during the 1998 survey.

A final comparison between all the survey periods for Netarts was made. The average lengths of the embayments are relatively equal for the 1997 and 2002 survey whereas the length of the embayments of the 1998 survey is larger. The average amplitudes of the embayments are larger for each successive survey period. The location of the center of the embayments is south of the center of the cell for 1997 and 2002 survey in contrast to the northern location in 1998. The maximum point of erosion is located in the northern portion of each embayment during the 1997 and 1998 survey while in the 2002 survey it is located in the southern end of the embayments. The locations of the embayments appears to be random for each survey and is shown in figure 15.

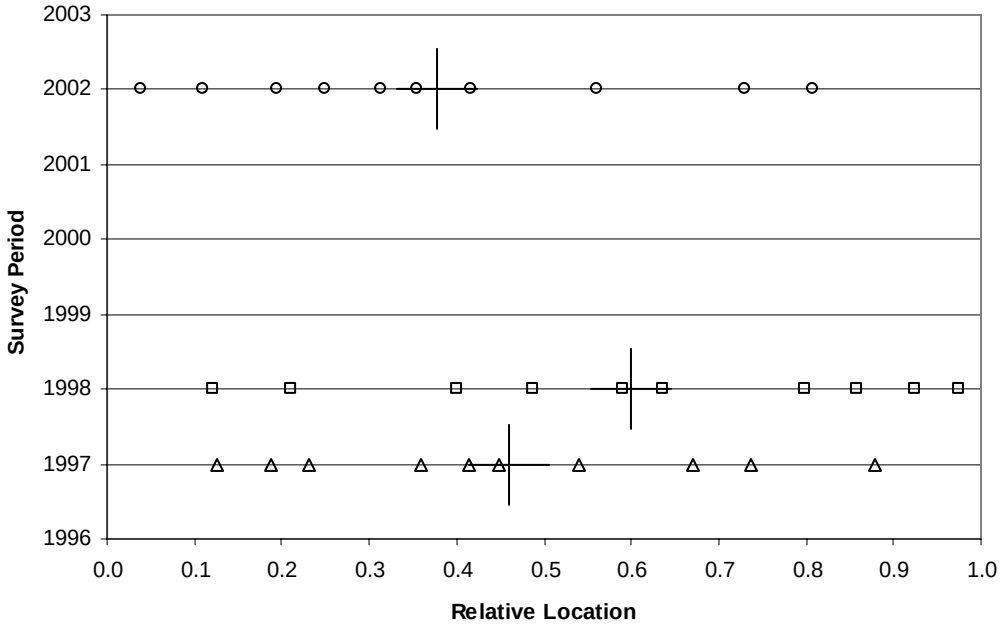

Figure 15 - Netarts sub-cell embayment location

4.2.4. Siletz Sub-cell

A total of 23 embayments were identified along the 7.73 km of the intermediate Siletz sub-cell from the 1998 and 2002 lidar survey data. A summary of these measurements are shown in table X. The average embayment length and amplitude within this sub-cell is 505 and 19 meters. The embayment length within this sub-cell is less than the overall average at 505 meter. The embayment amplitude within the Siletz sub-cell has a slightly larger average value of the amplitude of 19 meters. The average aspect ratio of the embayments is 32. The relative location of the embayments is located to the north of the study domain. In

1998 the embayments were skewed to the south while the 2002 embayments were on average near symmetrical.

Table 9 - Siletz sub-cell measurements

Measurement			1998	2002	Average
Beach Length		**[km]**	7.73	7.73	7.73
Embayment Count		**#**	13	10	11.5
Embayments/km		**[1/km]**	1.73	1.33	1.56
Mean Location		**-**	0.58	0.54	0.60
Spacing	**Average**	**[m]**	**553**	**686**	**611**
	Standard dev.	[m]	202	389	
Length	**Average**	**[m]**	**552**	**445**	**505**
	Standard dev.	[m]	201	117	
	Kurtosis	**-**	-1.39	-0.29	
Amplitude	**Average**	**[m]**	**23**	**15**	**19**
	Standard dev.	[m]	15	7	
	Kurtosis	**-**	1.18	-1.29	
Aspect Ratio	**Average**	**-**	**32**	**33**	**32**
	Standard dev.	**-**	18.06	9.88	
	Kurtosis	**-**	6.59	-1.56	
Skewness	**Average**	**-**	**-0.18**	**-0.01**	**-0.11**
	Standard dev.	**-**	0.27	0.36	
	Kurtosis	**-**	-1.34	-1.41	

Both the length and amplitude are reduced between surveys by 19% and 35% respectively. There is a slight 6% increase is the aspect ratio as a result of the differing length scales. The average relative location of the embayments is south of the 1998 survey but still to the north of the sub-cell center. There is no obvious correlation between the locations of the embayment points from the survey dates (Figure 17) 0

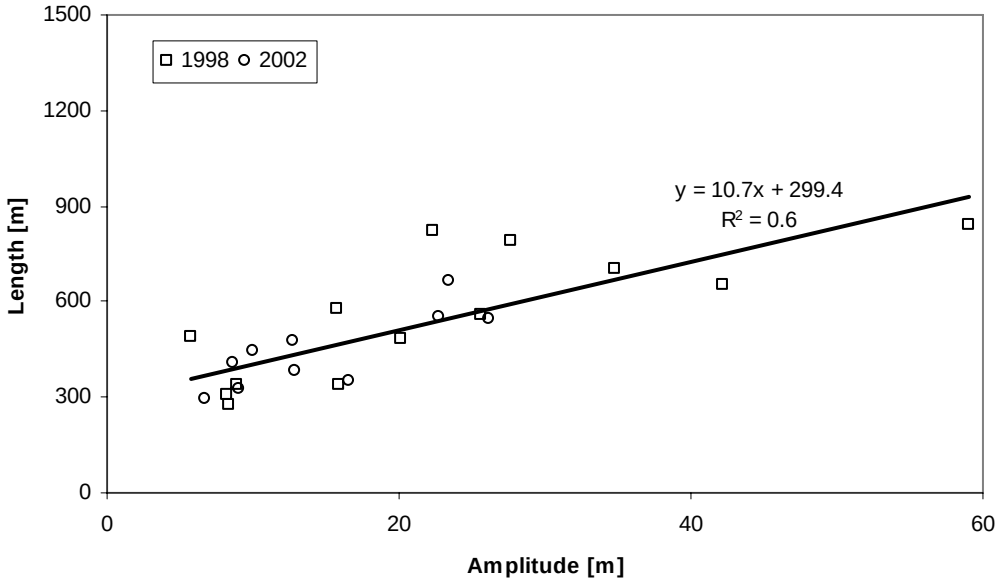

Figure 16 - Siletz sub-cell length/amplitude relation

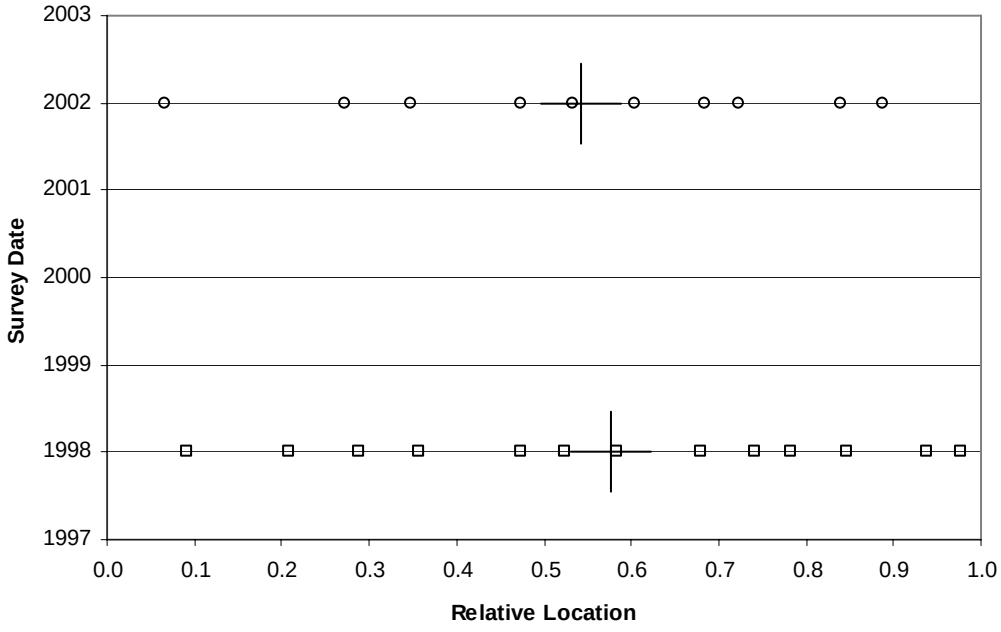

Figure 17 - Siletz sub-cell embayment location

4.3. Sub-cell comparison

Variability between the study sites is investigated by comparing the average values of each sub-cell for a given period. At any given survey period 10 to 13 embayments are located along a single study site. These embayments exhibit a wide range of features throughout each study locations and time period. For both the 1998 and 2002 lidar surveys average values of the morphological characteristics of the embayments are evaluated to try and find a dominant embayment signal specific to each.

The results from the 1998 lidar survey are compared (Table 10). The largest number of embayments is located on the Siletz sub-cell with a rate of 1.73 embayments per km having an average spacing of 553 meters. The smaller than average spacing is echoed in the smaller than average embayment length of 552 meters. With the smallest average length, the Siletz sub-cell has the largest average amplitude. This is reflected with the smallest aspect ratio. In addition, the embayment with the largest amplitude of 59 meters (840 meter length) is found within the 1998 lidar survey of Siletz. Siletz also differs in the average embayment skewness; with an average maximum point of erosion located within the southern portion of the embayment while this location is north of center in the remaining sub-cells. This sub-cell is different from the others because of a coarser grain size owing to a more intermediate profile unlike the dissipative profile of the additional study sites.

Table 10 - 1998 embayment comparison

Average Measurements		Nehalem	Rockaway	Netarts	Siletz
Beach Length	**[km]**	7.80	8.77	8.71	7.73
Embayment Count	**#**	10	12	10	13
Embayments/km	**[1/km]**	1.28	1.39	1.16	1.73
Mean Location	**[km/km]**	0.40	0.52	0.60	0.58
Spacing	**[m]**	666	677	815	553
Length	**[m]**	568	585	706	552
Amplitude	**[m]**	18	18	14	23
Aspect Ratio	**[m/m]**	36	46	53	32
Skewness	**[m/m]**	-0.04	0.05	0.04	-0.18

There are other notable differences between the sub-cells of the 1998 survey. Whereas the Siletz sub-cell has the shortest average length and largest average amplitude owing to a small aspect ratio, the inverse is found at the Netarts study site. Netarts has the largest average length at 706 meters with the smallest average amplitude of 14 meters during this study period. The results of the 1998 survey data are very similar between the two barring the average relative embayment location.

Results comparing the embayment for each sub-cell collected during the 2002 survey are shown in table 11. The Siletz sub-cell maintained two similarities with the previous survey; smallest average length and an inverse skewness. There are no apparent similarities between the 1998 and 2002 survey when comparing the sub-cell averages. During this survey period the Nehalem sub-cell had the most embayments per kilometer of beach length. This location also had the longest embayment recorded with a length of 1256 meters (45.2 meter amplitude). Netarts provided the largest average mean length of 691 meters while the embayments within the rockaway sub-cell have the largest average amplitude

Table 11 - 2002 embayment comparison

Average Measurements		Nehalem	Rockaway	Netarts	Siletz
Beach Length	**[km]**	7.80	8.77	8.71	7.73
Embayment Count	**#**	12	11	10	10
Embayments/km	**[1/km]**	1.54	1.27	1.16	1.33
Mean Location	**[km/km]**	0.48	0.48	0.38	0.54
Spacing	**[m]**	650	717	737	686
Length	**[m]**	596	691	590	445
Amplitude	**[m]**	22	24	15	15
Aspect Ratio	**[m/m]**	32	37	47	33
Skewness	**[m/m]**	-0.12	-0.20	-0.11	-0.01

A comparison between all embayments measured in each sub-cell is made using the linear relationship between the length and amplitude. From table 12 you can see that all but the Netarts sub-cell have reasonable R^2 values indicating a linear trend. Using this relationship, a prediction of the amount of beach length and possible dune length affected by an embayment with a minimum amplitude of 5 meters. This is made by inserting a value of 5 into the linear equation and the resulting lengths for each sub-cell are shown in table 12. The Netarts sub-cell appears to have the greatest length of affected beach per embayment but also has the worst linear relationship.

Table 12 – Length/amplitude relation comparison

Length-Amplitude Relationship L=C1*A+C2		Nehalem	Netarts	Rockaway	Siletz
C1	**[m/m]**	16.6	8.5	14.5	10.7
C2	**[m]**	252	520	335	299
R^2	**-**	0.7	0.1	0.8	0.6
L min	**[m]**	335	562	407	352

4.4. Sensitivity Analysis

The MHW tidal elevation is used in this study to define the shoreline. As previously shown in figure 3, rip current embayments are highly three dimensional and their measured morphology are dependant upon the selection of the datum. To investigate the affect that the datum has on embayment identification and length scales separate analysis was conducted using different vertical elevations.

The next highest tidal datum, mean high high water was used. The elevation of MHHW in Oregon is 2.25 meters, which is only 0.15 meters above MHW in Oregon (Weber et al., 2005). The same methods were used for MHHW datum. Again due to the elevated water levels during the 1997 survey the shorelines for Nehalem, Rockaway, and Siletz did not meet the 95% completeness threshold to be analyzed.

The results from the two tidal datums are presented in table 13. The average length at each location increased as expected. On average the amplitude is comparable to the MHW analysis. The number of embayments decreased except at the Nehalem cell. The reduction of the number of embayments is partially due to reduced amplitude of individual embayments to values less than the threshold value of 5 meters. The results are not very significant however they do follow the expected trend.

Table 13 - Sensitivity analysis of shoreline datum

Location	Datum	Embayment Count #	Avg Length [m]	Avg Amplitude [m]
Nehalem	**MHW**	11	583	20
	MHHW	11.5	600	19
Rockaway	**MHW**	11.5	636	21
	MHHW	9.5	727	25
Netarts	**MHW**	10	627	13
	MHHW	9.3	650	12
Siletz	**MHW**	11.5	505	19
	MHHW	11.5	516	19
ALL	**MHW**	**10.9**	**591**	**18**
	MHHW	**10.3**	**620**	**18**

This sensitivity analysis only considers and elevation change of 15 cm which is equal to the vertical error of the lidar data. This account for the slight change of length scales. To further pursue the sensitivity of the analysis an elevation of 3 meters is selected. Well defined embayments again increased in length and slightly in amplitude. Also, the less pronounced embayments did not meet the amplitude threshold criterion thus fewer embayments were identified. One additional affect is created by raising the shoreline elevation; false identification of embayments. Shoreline features similar to embayments are seen at the 3 meter contour however these features do not exist at lower elevations. Coastal streams that flow out though the beach are the main cause. The streams represent a topographical low. The three meter contour would follow the stream low into the dune region and appear as an embayment. A similar effect is caused in local regions where there is a low gap in the dune caused by a walk way or previous erosion.

Measurements of morphological features are not exact. Two main sources of error are inherent in measuring morphology; the precision of the measurement technique and the identification of the feature measured. Dependable measurements of morphologic features likely to be rip current embayments should be made at the lowest possible elevation on the beach face.

5. Discussion

Measurements calculated from the lidar surveys provide a snapshot of the sub-aerial coastal system. The state of the sub-aqueous morphology is unknown at the time of the survey. Only wave and tide measurements are continuously collected surrounding the survey periods, thus, it is difficult to provide a context of when, how, and why the surveyed morphology exists. Although limited by available data, answers to these questions are discussed.

5.1. Antecedent wave conditions

At any given time there were between 10 and 13 embayments at each of the study sites. Though conditions during the survey period were relatively equal, the antecedent wave conditions prior to each survey differ. Wave conditions four weeks prior to each survey consisting of significant wave height and dominant wave period are shown in figures 18 and 19. Prior to the 1997 and 1998 surveys sizable wave energy was recorded with events having a significant deep water wave height greater than 5 meters and existed around one week prior to the survey date. Prior to the 2002 survey calm conditions persisted with the last major storm event occurring nearly five months prior to the survey date.

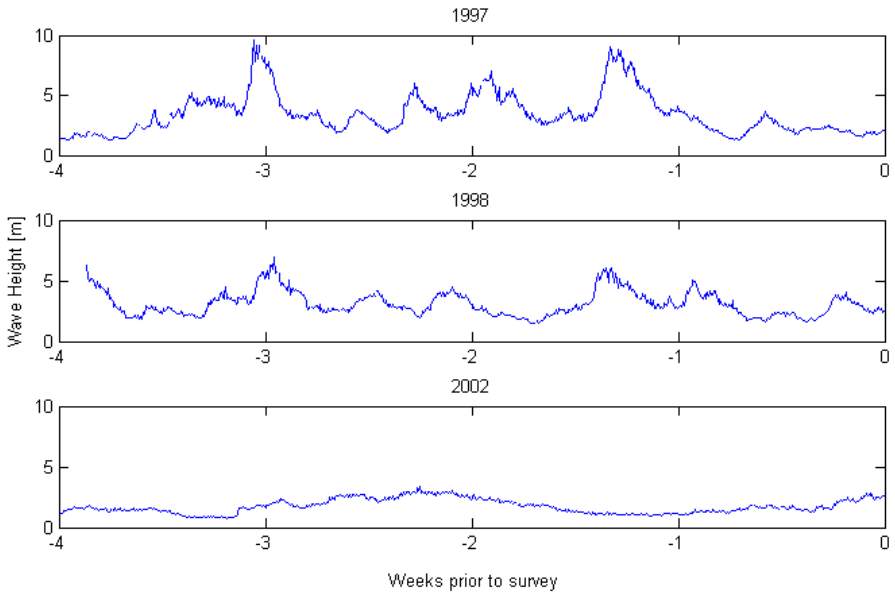

Figure 18 - Antecedent wave conditions 4 weeks prior to lidar surveys

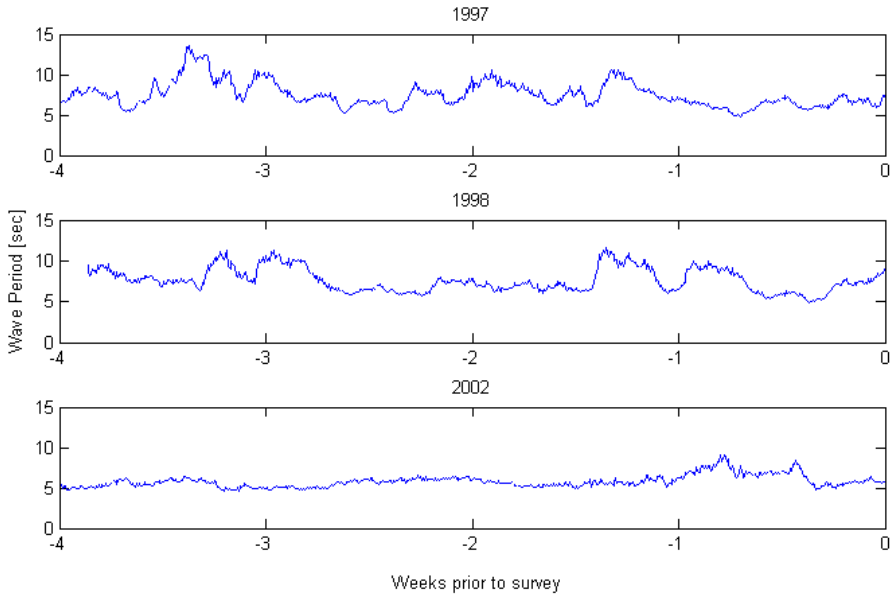

Figure 19 - Antecedent wave conditions - period

This discrepancy between the 1997 and 1998 antecedent wave conditions with the 2002 conditions does not explain differences within the embayment

results. The conditions necessary to create and erase rip current embayments in Oregon have not been documented. Observations of rip current embayment occurring in New Zealand are associated with spring tides with a mean wave height of 2.2 meters. These embayments had a undefined mean length of 120 meters occurring on a foreshore characterized by medium sand and a slope of ~0.06 (Shand04). Conditions, similar to those preferred in New Zealand, exist for ~1 week between the last major storm and the survey dates for the 1997 and 1998 surveys. The average embayment size from the 1997 and 1998 surveys for this study is O (100's meters). There is no known data of features of this magnitude forming in this time period. The effects of the storm events prior to the survey are unknown.

5.2. Migration during El Niño

Without the knowledge of thresholds necessary to generate or destroy embayments it is difficult to determine if each embayment is unique with respect to time. This problem arose when analyzing the embayments located on the Netarts sub-cell during the 1997 and 1998 lidar surveys. These surveys were taken 7 months apart without an intermittent survey. At each survey period an equal number of embayments were observed.

When comparing the locations of each embayment between these two years there was not an obvious correlation in the locations of embayments. Although migration of individual embayments has been observed (Komar et al., 1989; Thornton et al., 2007) in the past, for this data, there does not appear to be a

consistent migration pattern. It is believed that the embayments would all migrate to the north during an El Nino winter. There was a shift of the mean location to the north, however the locations of individual embayments are not north of the 1997 survey. It is possible that some embayments lasted through the winter, migrated and possibly merged (Stephens et al., 1999).

5.3. Variability of the embayments

In general, there appears to be a linear relationship between the lengths and amplitudes of the embayments (Figures 9, 10, 12, 14, 16 and Table 12). The varying sizes of embayments are thought to be caused by the varied strengths and size of circulation cells located within the surfzone. A linear regression provides a relationship between the length and amplitude of the different embayments. Steep slopes indicate relatively equal amplitudes with varying length while flat slope indicate relatively equal lengths with varying amplitudes. It is possible that the trend line represents the growth path for embayments located within a certain beach. This trend line may also provide a length and amplitude relationship limit to embayments. Taking the linear relationship, a minimum length of an embayment with the minimum 5 meters of amplitude can be calculated.

The aspect ratio relates the embayment length of the embayment to its amplitude. It is believed that the degree of storm erosion in the presence of embayments is dependant on the aspect ratio. Embayments with large aspect ratios do not provide a large amount of beach width reduction. Where as embayments with a lower aspect ratio provide more beach width reduction for a

given length. Similar to the linear relationship there is most likely a lower and upper bound of the aspect ratio relative to embayments.

5.4. Embayment slope relationship

The lidar data indicates a relation between the shoreline slope and the embayment location. Locations of maximum points of erosion correspond with locations of maximum slope, opposite that of smaller beach cusps. This relationship is seen when the MHWbp filtered shoreline (solid line) and slope (dashed line) are plotted in the alongshore on a separate vertical axis in figure 20 where the vertical lines are the embayment locations. This relationship was seen for all study sites.

A definite explanation for the increase of slope within the embayment is unknown. Rip embayments can cause scarps on the beach face of O(1 meter) and the scarp may be within the range of the slope calculation. A variation in grain size through the embayment may account for this variability. If sediment size increases towards the most erosive point of the embayment a steeper beach profile may exist. This type of sorting might be caused during the erosion of the embayment where the fines are first removed.

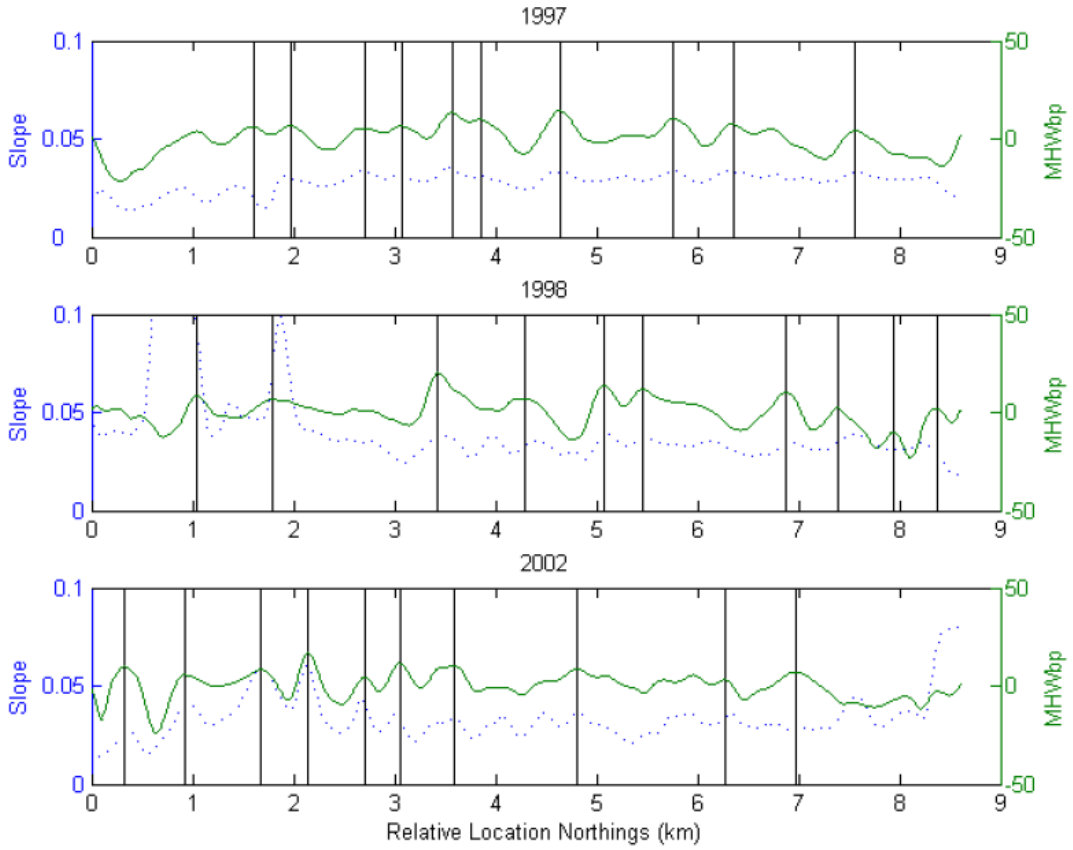

Figure 20 – Embayment/slope relationship - Netarts sub-cell

5.5. Sediment Size Dependence

Results from the Siletz sub-cell indicate that there is a dependence between the beach profile and sediment size. The Siletz sub-cell differs from the other sub-cells with its coarser sand grains and more intermediate beach profile. While the amplitudes of the embayments within this location are comparable to the other sub-cell the average length is noticeably smaller. It is unknown why a coarser sand grain would cause the embayments to have a smaller aspect ratio.

6. Embayment Modeling

Rip current embayments are thought to exist as a result of an interaction between the nearshore hydrodynamics and the beach. By definition a rip current embayment involves a rip current. The features that have been found in this study are akin to rip embayments but there is no proof that these embayments were in fact caused by rip currents or that rip currents exist within embayments. Measuring the hydrodynamics within a rip current embayment found in Oregon is difficult and dangerous and thus, such data does not exist. To provide insight as to whether a rip current exists in an embayment and if so, under what conditions, the numerical circulation model SHORECIRC is used to provide simulations.

SHORECIRC is a quasi 3-D nearshore circulation model. In this study it calculates long-term, time-averaged, depth-averaged, current velocities. From these velocity values rip currents are identified. Locations of rip currents are defined as having a cross-shore velocity greater than 0.10 m/s extending beyond the surf zone.

6.1. Bathymetry

SHORECIRC requires bathymetry as an input. The morphology of rip current embayments in Oregon have not been surveyed in detail. Using the results of the lidar measurements, anecdotal evidence, and general characteristics of the Oregon coastline an idealized bathymetry of a rip embayment is created.

The bathymetry is created on a uniform grid with 5 meter spacing in both the cross-shore and longshore. Generation of the bathymetry is based on the equilibrium beach profile equation, $y=Ax^m$. Y is water depth, x is cross-shore location, A is a dimensionless parameter, and m is a dimensionless exponent. A controls the overall steepness of the profile whereas m controls the profile shape (Masselink and Hughes, 2003).

A symmetric embayment with a width and amplitude of 575 and 17 meters is placed within a straight shoreline with a constant equilibrium beach profile figure 21. The bathymetry extends from a depth of 0 to a depth of 6.2 meters in the offshore and extends 1150 meters in the alongshore. The constant equilibrium profile of the non-embayed beach have values of A = 0.09 $m^{1/3}$ and m = 0.64. With a common grains size of 0.2 mm for Oregon the value of A is reasonable from (Dean et al., 1994).

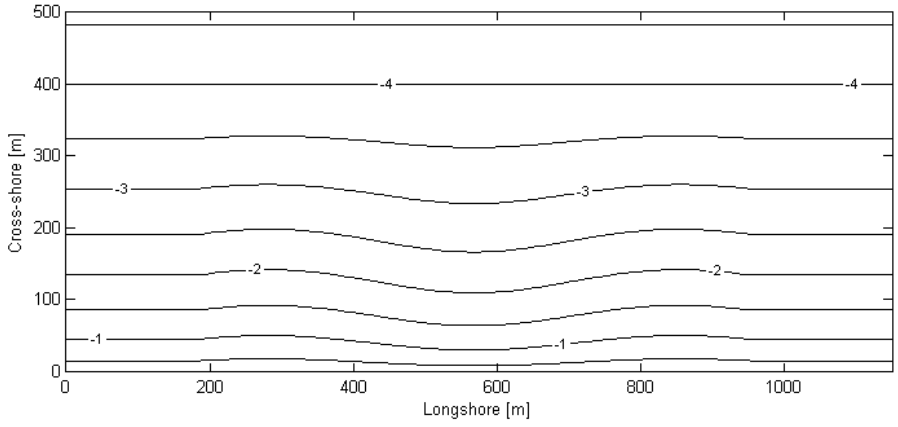

Figure 21 - Embayment bathymetry plan view

The embayment is created by varying the A and m parameters in the longshore. Variation of m is created by using a component of the sin function. Values of m range from 0.54 within the embayment center to 0.67 on the horns surrounding the embayment (Figure 22). Discontinuity in the offshore is avoided by setting offshore limits of the profile affected by the embayment to 400 meters in the cross-shore with a depth of 4 meters, thus providing a common point for all profiles. With the cross-shore distance and depth at the shoreline and offshore set at (0, 0) and (400, 4), and a value of m for each profile the value of A is solved for. Values of A range from 0.16 at the embayment to 0.07 at the horns. Beyond 400 meters in the cross-shore the profiles are uniformly extended to 800 meters where the depth is 6.2 meters.

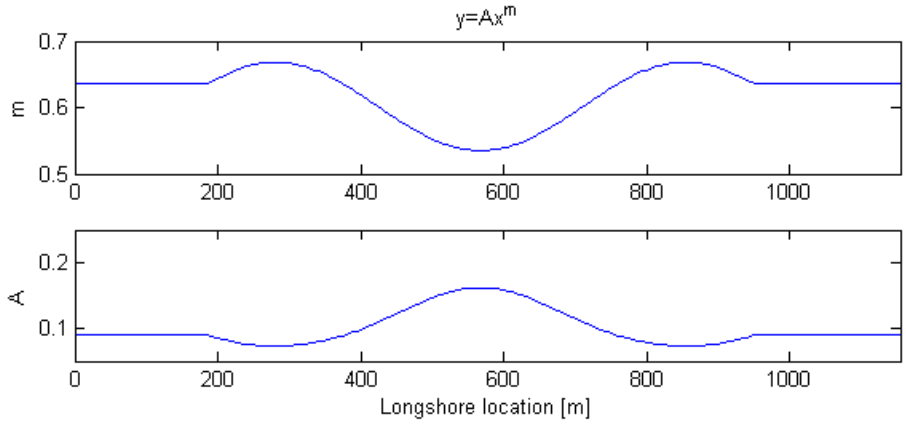

Figure 22 - Equilibrium beach profile dimensionless parameters

Values for the dimensionless A parameter have been empirically related to sediment fall velocity and thus grain size. Dean (1987) provides the relationship between A and the sediment fall velocity w_s in cm/s and fall velocity has been

related to sediment characteristics by Gibbs et al. (1971). Using their empirical formula fall velocities and grain size can be back-calculated. The results of these calculations are shown in figure 23.

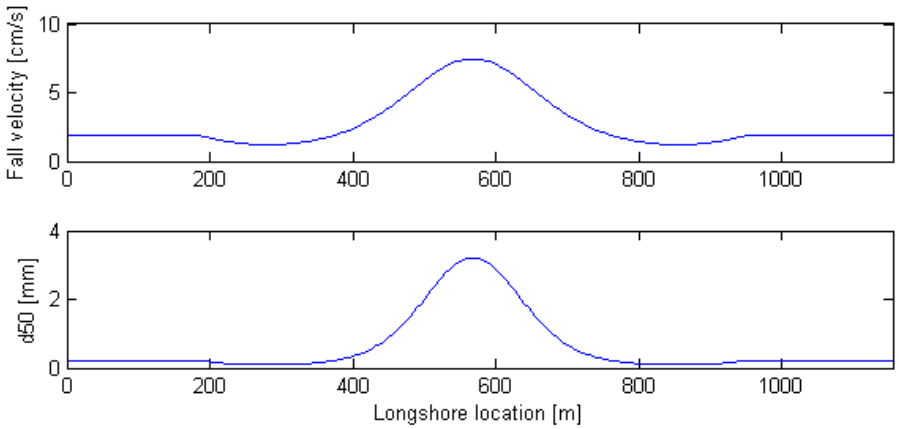

Figure 23 – Back-calculations of sediment characteristics

The variation of these parameters creates an embayment that has an amplitude that varies with offshore location which is indicated by figure 24. The amplitude varies from zero at the shoreline and embayment limits to a maximum of 33 meters. The elevation where the amplitude is equal to 18 meters, the average embayment amplitude form the lidar study, is -0.84 meters. This elevation is representative of the MHW contour from our lidar study.

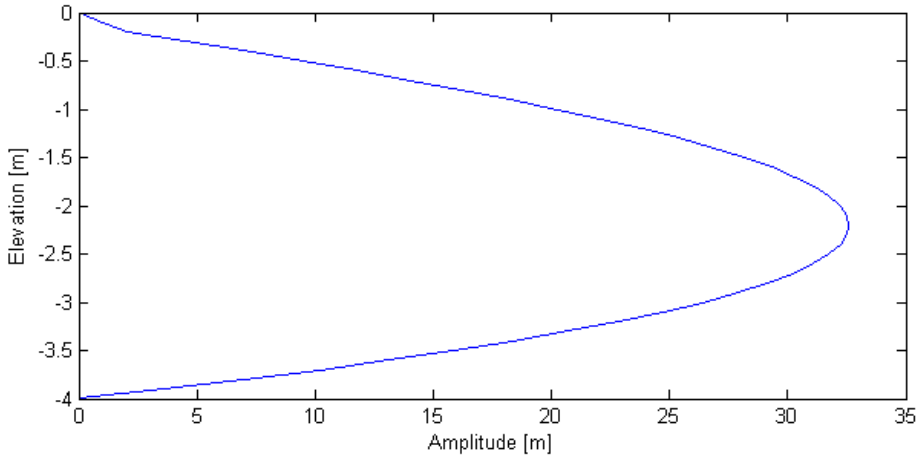

Figure 24 - Embayment amplitude

6.2. Model Conditions

A total of three model runs are used to examine the hydrodynamics within the idealized rip current embayment using SHORECIRC. All variables are held constant except for the initial wave condition. A summary of the input conditions are located in the Appendix.

The created bathymetry is symmetric and periodic boundary conditions are placed in the longshore. The shoreline is represented as a wall in the model. It is necessary to maintain a minimum water depth at the wall and it is placed 10 meters from the initial shoreline. The wall also prevents water landward of its location. The water level during the model runs is at an elevation of 0, thus the equivalent model MHW of -0.84 meters is submerged during the simulations. Wave generation is located at the offshore boundary, x = 800 meters.

Wave heights are input into REF/DIF via indat.dat and shoaled from the offshore boundary. The wave heights used are 1, 2, and 3 meters and approximately represent summer, yearly and winter mean wave heights, respectively. The wave period is held constant during at 9 seconds. The monochromatic waves have an angle of zero, and approach the shoreline normally at the offshore model boundary. Wave breaking is depth limited in this model and there is no wave current interaction.

Each model run is 5000 seconds. This provides ample length for the rip current to become quasi-stable. Long-term averaged values are calculated starting after a 100 second delay. This removes time varying fluctuation in the circulation.

6.3. Results and Discussion

The model simulations indicate that rip currents can exist within an idealized rip current embayment morphology. The results from the simulations are shown in figures 25-30. For each wave condition there are two figures; one containing the magnitude of the currents and a second with the direction of the currents and the locations of rip currents. The rip currents are identified by searching for cross-shore velocities greater than 0.1 m/s outside of the surf zone. The surf zone, bold dashed line is found in the alongshore as the maximum wave height.

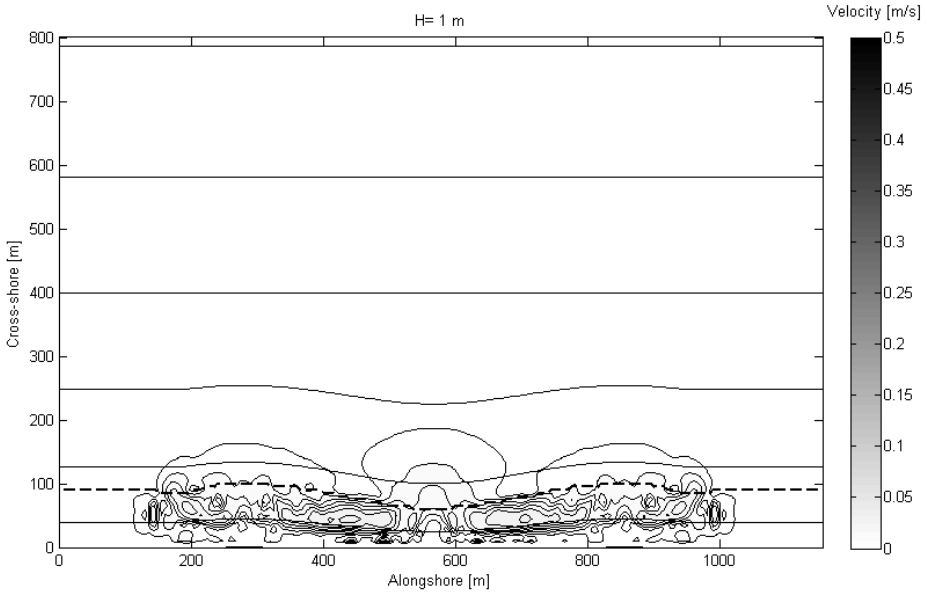

Figure 25 – H = 1 meter – current velocity

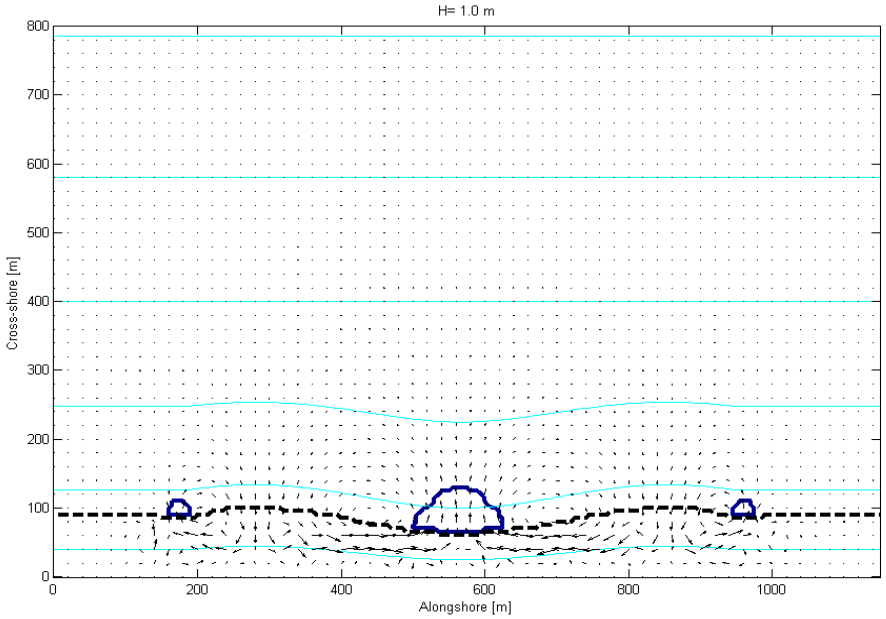

Figure 26 – H = 1 meters – location of rip currents

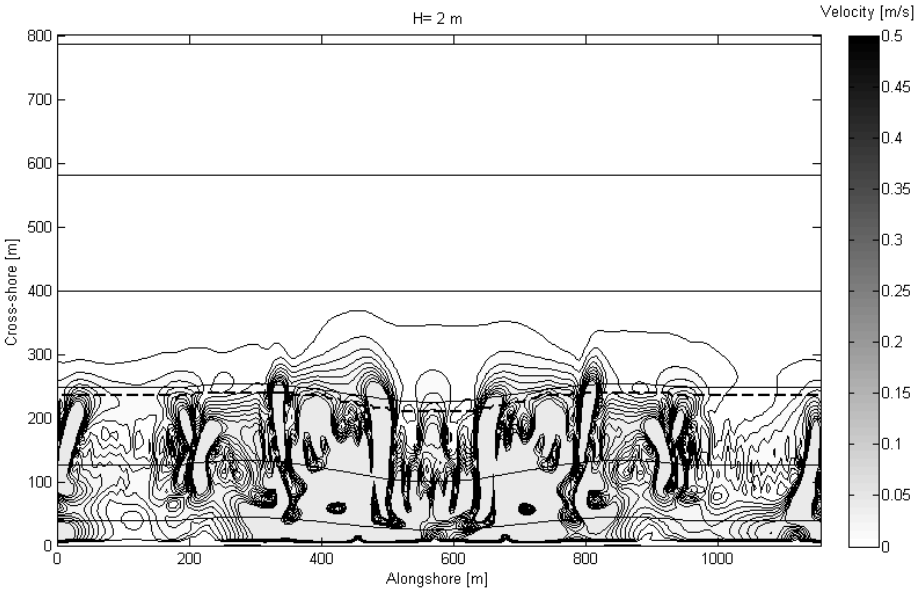

Figure 27 - H = 2 meters - current velocity

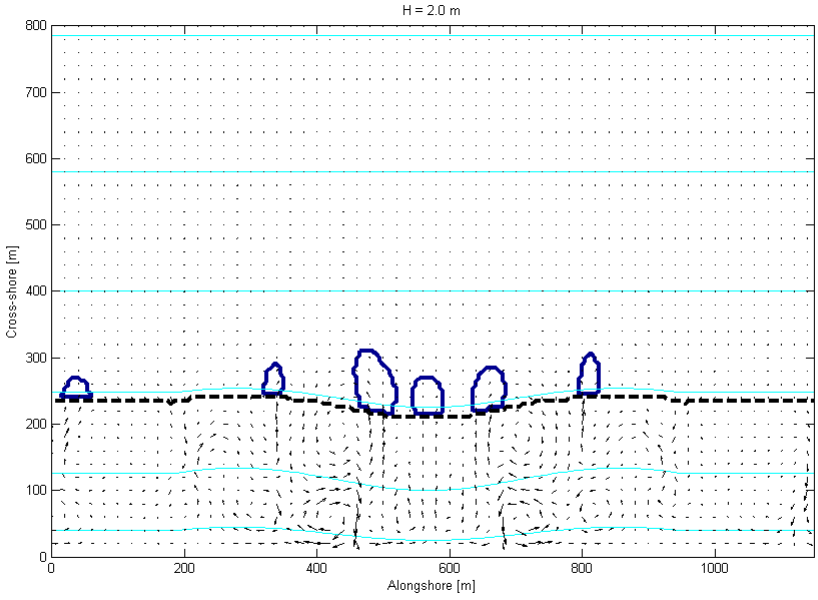

Figure 28 – H = 2 meters – location of rip currents

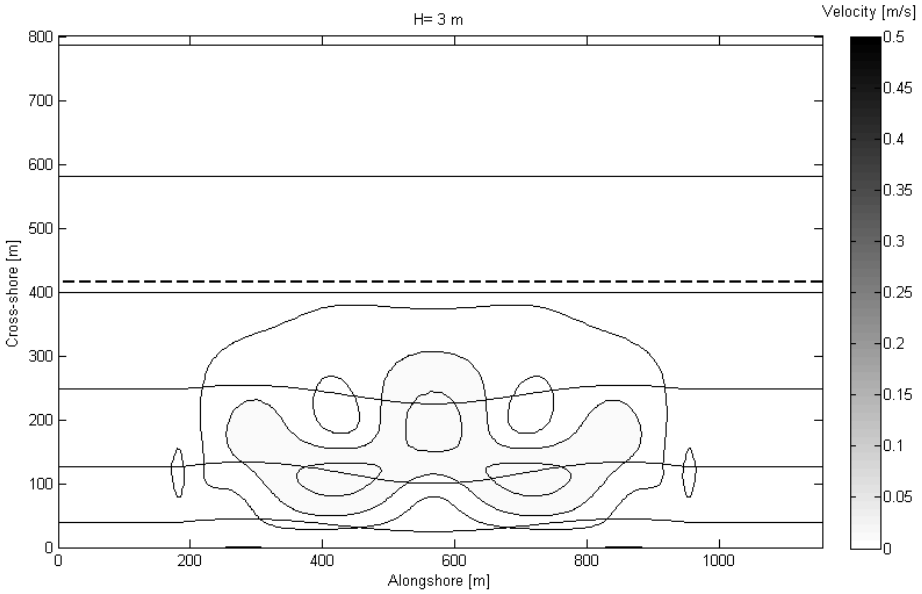

Figure 29 - H = 3 meters - current velocity

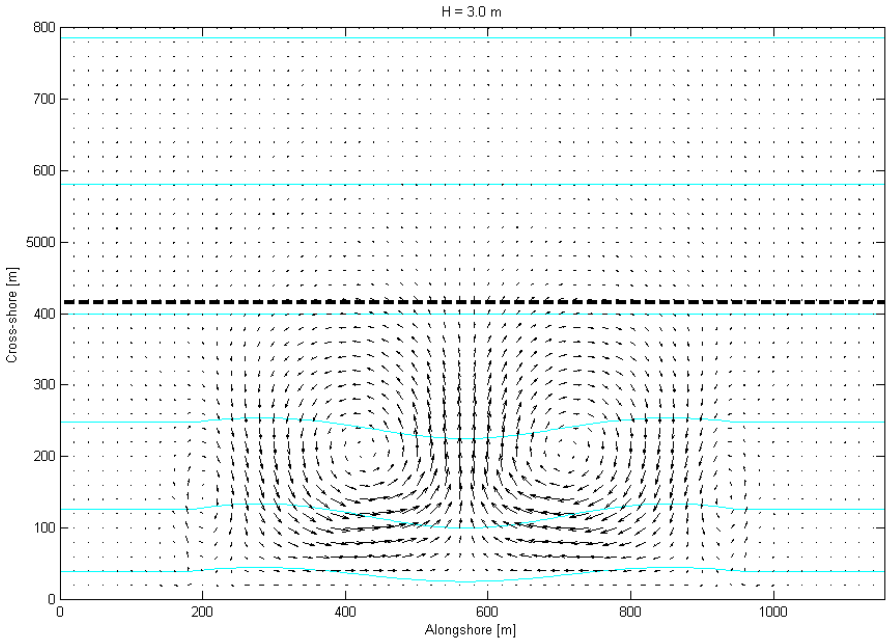

Figure 30 – H = 3 meters – location of rip currents

Circulation patterns indicative of rip currents exist for all three wave conditions. However, according to our definition that rip currents are located where the cross-shore velocity is greater than 0.1 m/s outside of the surf zone, only the 1 and 2 meter wave conditions produce rip currents. Circulation patterns vary with each wave condition. A single central rip current with velocities ~17cm/s is created under 1 meter wave conditions. This current is fed by two feeder currents within the surfzone that extend to the embayment horns. Under the 2 meter wave condition multiple rip currents form within the embayment. The magnitudes of the velocities within these rip are ~50 cm/s. There are no defined feeder currents. Under the 3 meter wave condition there is a clean circulation pattern with velocity magnitudes ~15cm/s. Under this wave condition the surf zone is ~400 meters wide due to the highly dissipative profile and the currents do not extend beyond it. Although it does not extend beyond the surf zone the circulation pattern is consistent with rip currents.

7. Conclusions

A method is presented to extract morphological features nalogous to rip current embayments, with length ranging from 100-1500 meters and amplitudes greater than 5 meters, from a datum based shoreline contour. For this study the operational Oregon MWH tidal datum was used to define the shoreline. The shoreline contour was established from lidar data of the Oregon coastline collected during 1997, 1998, and 2002. Shoreline variability within the defined length range is exposed by bandpass filtering the shoreline. Resulting shoreline features are extracted and their critical points identified using a multiple maximum-minimum method. Measured features having a minimum length and amplitude of 100 and 5 meters, respectively, are deemed plausible rip current embayments.

Individual morphological measurements are calculated using the location of the embayment horns and the most erosive point of the embayment. These measurements include the length, amplitude, skewness, and aspect ratio. Additional calculations are made to try and identify spatial and temporal relationships. These measurements are the relative embayment locations, embayment spacing, quantity of embayments, and a linear length-amplitude fit.

A total of 98 individual embayments were extracted from ~75 km of beach. The average length and amplitude of the embayments are 591 and 18 meters, respectively. Each embayment is unique and has its own shape which is described by the aspect ratio and skewness, and the average embayment has an aspect ratio

of 41 and is nearly symmetric. The characteristics of embayments in Oregon are much larger than those found elsewhere in the world.

The embayments affect a major portion of each sub-cell. The total length of the embayments consists of 77% of the total beach length. The locations of these embayments are random and the mean location of the embayments is near the center each sub-cell.

Using the lidar results an idealized bathymetry of a rip current embayment was created for modeling. Based on this bathymetry, SHORECIRC, a nearshore circulation model was used to investigate the presence of rip currents within the embayments due to wave heights of 1, 2 and 3 meters and wave period of 9 seconds. The 1 and 2 meter wave conditions created rip currents within the embayment with cross-shore velocities exiting the surfzone larger than 10 cm/s. A circulation pattern similar to rip currents was created with the 3 meter wave conditions however the currents did not exit the surf zone.

From this research it has been observed that rip current embayments are a major morphological feature of the Oregon coastline. The location and size of these embayments are of O (600 meters) and provide the potential for localized erosion of dunes and cliffs, thus are very hazardous features.

Further research is necessary to understand to formation and evolution of rip current embayments so that their location and size may be predicted. Continued modeling of an idealized bathymetry can provide more insight into the

hydrodynamics involved with embayments; however without field measurements these model predictions have not been proven. We believe that a detailed field study consisting of detailed morphologic and hydraulic measurements is necessary to further advance the research of rip current embayments in Oregon.

Bibliography

Aagaard, T.; Greenwood, B. & Nielsen, J. (1997), 'Mean currents and sediment transport in a rip channel', *Marine Geology* **140**, 25-45.

Allan, J. & Komar, P. (2002), 'Extreme storms in the Pacific Northwest coast during the 1997-98 El Nino and 1998-99 La Nina', *Journal of Coastal Research* **18 (1)**, 175-193.

Allan, J.C.; Komar, P.D. & Priest, G.R. (2003), 'Shoreline variability on the high-energy Oregon Coast and its usefulness in erosion-hazard assessments', *Journal of Coastal Research* **SI 38**, 83-105.

Allan, J. (2006), 'Rockaway beach survey', *http://www.oregongeology.com/sub/Nanoos1/index.htm.*

Blondeaux, P. (2001), 'Mechanics of coastal forms', *Annual Review Fluid Mechanics* **33**, 339-370.

Boak, E. & Turner, I. (2005), 'Shoreline definition and detection: a review', *Journal of Coastal Research* **21**, 688-703.

Brander, R.W. & Cowell, P.J. (2003), 'A trend-surface technique for discrimination of surf-zone morphology: Rip current channels', *Earth Surface Processes and Landforms* **28**, 905-918.

Clemens, K.E. & Komar, K. (1988), 'Oregon beach sands compositions producing the mixing of sediments under a transgressing sea', *Journal of Sedimentary Petrology* **58 (3)**, 519-529.

Cook, D.O. (1970), 'The occurrence and geologic work of rip currents off Southern California', *Marine Geology* **9**, 173-186.

Dean, R.G., T.L. Walton, and D.L. Kriebel, “Cross-shore sediment transport,” in *Coastal Engineering Manual*, U.S. Army Coastal and Hydraulics Laboratory, 2001.

Dolan, R. (1971), 'Coastal landforms: crescentic and rhythmic', *Geological Society of America Bulletin* **82**, 177-180.

Dean, R.G. (1987),Coastal sediment processes: toward engineering solutions, *in* 'Coastal Sediments '87, ASCE'.

Gibbs, R.J.; Matthews, M.D. & Link, D.A. (1971), 'The relationship between sphere size and settling velocity', *Journal of Sedimentary Petrology* **41**, 7-18.

Holman, R.A.; Symonds, G.; Thornton, E.B. & Ranasinghe, R. (2006), 'Rip spacing and persistence on an embayed beach', *Journal of Geophysical*

Research **111**, C01006.

Komar, P.D. (1971), 'Nearshore cell circulation and the formation of giant cusps', *Geological Society of America Bulletin* **82**, 2643-2650.

Komar, P.D. & Rea, C.C. (1976), 'Erosion of Siletz Spit, Oregon', *Shore and Beach* **44**, 9-16.

Komar, P.D. (1983), *Mega-Geomorphology*, Clarendon Press, Oxford, chapter Rhythmic shoreline features and their origins, pp. 92-112.

Komar, P.D.; Good, J.W. & Shih, S. (1989), 'Erosion of Netarts Spit, Oregon: continued impacts of the 1982-83 El Nino', *Shore and Beach* **56**, 11-19.

Koptenko, S. (2003), 'Multiple maximum/minimum', *http://www.mathworks.com/matlabcentral/fileexchange/loadFile.do?objectId=3170*.

Krabill, W.B.; Thomas, R.H.; Martin, C.F.; Swift, R. & Frederick, E. (1995), 'Accuracy of airborne laser altimetry over Greenland ice sheet', *International Journal of Remote Sensing* **16**, 1211-1222.

Kraus, N.C. & Galgano, F.A. (2001), 'Beach erosional hot spots: types, causes, and solutions', *US Army Corps of Engineers ERDC/CHL CHETN-ll-44*.

List, J.H.; Farris, A.S. & Sullivan, C. (2006), 'Reversing storm hotspots on sandy beaches: spatial and temporal characteristics', *Marine Geology* **226**, 261-279.

MacMahan, J.H.; Thornton, E.B.; Stanton, T.P. & Reniers, J. (2005), 'RIPEX: observations of a rip current system', *Marine Geology* **218**, 113-134.

MacMahan, J.H.; Thornton, E.B. & Reniers, J.H.M. (2006), 'Rip current review', *Coastal Engineering* **53**, 191-208.

Masselink, G. & Hughes, M.G. (2003), *Introduction to coastal processes and geomorphology*, Oxford University Press Inc., New York.

McNinch, J.E. (2004), 'Geologic control in the nearshore: shore-oblique sandbars and shoreline erosional hotspots, Mid-Atlantic- Bight, USA', *Marine Geology* **211**, 121-141.

Morton, R.A.; Gibeaut, J.C. & Paine, J. (1995), 'Meso-scale transfer of sand during and after storms: implications for prediction of shoreline movement', *Marine Geology* **126**, 161-179.

Murray, A.B. (2004), 'Rip channel development on nonbarred beaches: the importance of a lag in suspended-sediment transport', *Journal of Geophysical Research* **109**.

NOAA (2007a), 'Lidar data', *http://www.csc.noaa.gov/crs/tcm/*.

NOAA (2007b), 'Tides Online', *http://tidesonline.nos.noaa.gov/*.

NOAA (2007c), 'National Data Buoy Center', *http://www.ndbc.noaa.gov/*.

Oregon Coastal Atlas (2007), '', *http://www.coastalatlas.net/index.asp*.

Revell, D.L.; Komar, P.D. & Jr., A.H.S. (2002), 'An application of LIDAR to analyses of El Nino erosion in the Netarts Littoral Cell, Oregon', *Journal of Coastal Research* **18**(3), 792-801.

Robertson, W.; Whitman, D.; Zhang, K. & Leatherman, S.P. (2004), 'Mapping shoreline position using airborne laser', *Journal of Coastal Research* **20**(3), 884-892.

Rogers, S. & Nash, D. (2003), *The dune book*, North Carolina Sea Grant.

Ruggiero, P.; Kaminsky, G.M.; Gelfenbaum, G. & Voigt, B. (2005), 'Seasonal to interannual morphodynamics along a high-energy dissipative littoral cell', *Journal of Coastal Research* **21, No. 3**, 553-578.

Sallenger, A.H.J.; Krabill, W.B.; Swift, R.N.; Brock, J.; List, J.; Hansen, M.; Holman, R.A.; Manizade, S.; Sontag, J.; Meredith, A.; Morgan, K.; Yunkel, J.K.; Frederick, E.B. & Stockdon, H. (2003), 'Evaluation of airborne topographic lidar for quantifying beach change', *Journal of Coastal Research* **19**, 125-133.

Seymour, R.J. (1998), 'Effects of El Nino in the West Coast wave climate', *Shore and Beach* **66 (3)**, 3-6.

Shand, R.; Hesp, P. & Shepherd, M. (2004), 'Beach cut in relation to net offshore bar migration', *Journal of Coastal Research* **SI 39**.

Shepard, F.; Emery, K. & Fond, E.L. (1941), 'Rip currents: a process of geological importance', *The Journal of Geology* **49, No. 4**, 337-369.

Stauble, D.K. & Gravens, M.B. (2004), 'Identification of and remedial approaches to hot spots', *Army Corps of Engineers ERDC/CHL CHETN-ll-47*.

Stephens, S.; Healy, T.; Black, K. & Lange, W. (1999), 'Arcuate duneline embayments, infagravity signals, rip currents and wave refraction at Waihi Beach, New Zealand', *Journal of Coastal Research* **Vol. 15, No. 3**, 823-829.

Stockdon, H.F.; Jr., A.H.S.; List, J.H. & Holman, R.A. (2002), 'Estimation of shoreline position and change using airborne topographic lidar data', *Journal of Coastal Research* **18**(3), 502-513.

Thronton, E.B.; MacMahan, J. & Jr., A.H.S. (2007), 'Rip currents, mega-cusps, and eroding dunes', *Marine Geology* **240**, 151-167.

Weber, K.M.; List, J.H. & Morgan, K.L.M. (2005), 'An operational mean high water datum for determination of shoreline position from topographic lidar', *U.S. Gelogical Survey Open-File Report 2005-1027*.

Wright, L.; Chappell, J.; Thom, B.; Bradshaw, M. & Cowell, P. (1979), 'Morphodynamics of reflective and dissipative beaches and inshore systems: Southeastern Australlia', *Marine Geology* **32**, 105-140.

APPENDIX

A. Lidar Results

Table 1 – Nehalem Sub-cell 1998

Embayment	Relative Location	Length	Amplitude	Aspect Ratio	Skewness
--	--	[m]	[m]	--	--
1	0.06	685	26	26	-0.22
2	0.13	673	26	25	0.24
3	0.20	381	7	52	0.22
4	0.28	547	23	24	-0.32
5	0.32	370	8	48	0.28
6	0.38	476	14	35	-0.09
7	0.45	560	11	49	0.03
8	0.64	675	25	27	-0.30
9	0.75	611	15	40	-0.08
10	0.83	702	24	30	-0.12
Mean	**0.40**	**568**	**18**	**36**	**-0.04**
Std	**0.26**	**124**	**8**	**11**	**0.22**
Kurt	**-0.97**	**-1.06**	**-1.87**	**-1.64**	**-1.38**

Table 2 - Nehalem sub-cell 2002

Embayment	Relative Location	Length	Amplitude	Aspect Ratio	Skewness
--	--	[m]	[m]	--	--
1	0.05	861	46	18.6	-0.02
2	0.17	266	5	50.1	-0.06
3	0.20	425	17	25.6	0.31
4	0.27	459	26	17.5	-0.25
5	0.33	346	7	46.3	-0.35
6	0.39	455	20	23.1	0.17
7	0.50	805	17	46.8	-0.48
8	0.57	515	16	31.5	-0.19
9	0.64	810	19	41.9	0.18
10	0.81	1256	45	27.8	-0.39
11	0.90	569	26	22.1	0.02
12	0.97	386	13	30.7	-0.36
Mean	**0.48**	**596**	**22**	**31.8**	**-0.12**
Std	**0.30**	**284**	**13**	**11.58**	**0.26**
Kurt	**-1.09**	**1.26**	**0.58**	**-1.37**	**-1.19**

Table 3 - Rockaway sub-cell 1998

Embayment	Relative Location	Length	Amplitude	Aspect Ratio	Skewness
--	--	[m]	[m]	--	--
1	0.07	422	12	35	-0.12
2	0.12	634	26	24	0.18
3	0.20	1092	41	27	0.32
4	0.37	1061	54	20	-0.40
5	0.44	552	18	31	0.06
6	0.50	479	12	40	0.12
7	0.55	610	6	110	0.30
8	0.66	400	8	52	-0.01
9	0.77	455	6	71	-0.72
10	0.78	335	5	66	0.64
11	0.84	542	12	44	0.19
12	0.93	442	16	28	0.01
Mean	**0.52**	**585**	**18**	**46**	**0.05**
Std	**0.29**	**245**	**15**	**26**	**0.35**
Kurt	**-1.19**	**1.36**	**1.91**	**2.49**	**1.37**

Table 4 - Rockaway sub-cell 2002

Embayment	Relative Location	Length	Amplitude	Aspect Ratio	Skewness
--	--	[m]	[m]	--	--
1	0.09	359	6	61	-0.53
2	0.14	479	7	74	-0.73
3	0.18	895	41	22	0.29
4	0.35	1155	33	35	-0.61
5	0.40	633	18	35	0.31
6	0.47	294	7	44	-0.19
7	0.54	705	21	33	0.23
8	0.64	638	25	26	-0.22
9	0.73	790	22	37	-0.38
10	0.82	989	57	17	-0.24
11	0.91	662	27	25	-0.16
Mean	**0.48**	**691**	**24**	**37**	**-0.20**
Std	**0.28**	**260**	**16**	**17**	**0.36**
Kurt	**-1.16**	**-0.34**	**0.64**	**0.99**	**-1.03**

Table 5 - Netarts sub-cell 1997

Embayment	Relative Location	Length	Amplitude	Aspect Ratio	Skewness
--	--	[m]	[m]	--	--
1	0.13	775	5	142	-0.60
2	0.19	567	6	97	-0.36
3	0.23	570	7	81	0.31
4	0.36	453	6	81	0.03
5	0.42	438	9	47	-0.19
6	0.45	534	5	105	0.62
7	0.54	773	21	38	0.01
8	0.67	569	12	47	0.09
9	0.74	494	9	57	-0.02
10	0.88	688	10	72	0.11
Mean	**0.46**	**586**	**9**	**77**	**0.00**
Std	**0.25**	**122**	**5**	**32**	**0.34**
Kurt	**-0.90**	**-0.85**	**4.38**	**0.47**	**0.76**

Table 6 - Netarts sub-cell 1998

Embayment	Relative Location	Length	Amplitude	Aspect Ratio	Skewness
--	--	[m]	[m]	--	--
1	0.12	547	13	43	-0.31
2	0.21	1080	11	98	0.23
3	0.40	919	29	31	0.25
4	0.49	715	10	75	0.53
5	0.59	528	17	31	-0.36
6	0.64	1181	14	82	0.63
7	0.80	720	18	40	-0.26
8	0.86	635	11	59	0.26
9	0.92	325	9	36	-0.06
10	0.98	411	11	39	-0.48
Mean	**0.60**	**706**	**14**	**53**	**0.04**
Std	**0.30**	**280**	**6**	**24**	**0.39**
Kurt	**-1.08**	**-0.69**	**3.95**	**-0.54**	**-1.46**

Table 7 - Netarts sub-cell 2002

Embayment	Relative Location	Length	Amplitude	Aspect Ratio	Skewness
--	--	[m]	[m]	--	--
1	0.04	554	29	19	0.03
2	0.11	589	16	37	-0.12
3	0.20	755	15	51	-0.32
4	0.25	535	25	21	0.14
5	0.31	378	10	39	-0.30
6	0.35	427	14	30	-0.05
7	0.42	572	14	41	-0.19
8	0.56	749	8	100	-0.52
9	0.73	321	6	56	0.18
10	0.81	1017	14	75	0.01
Mean	**0.38**	**590**	**15**	**47**	**-0.11**
Std	**0.26**	**206**	**7**	**25**	**0.22**
Kurt	**-0.69**	**0.79**	**0.36**	**1.12**	**-0.43**

Table 8 - Siletz sub-cell 1998

Embayment	Relative Location	Length	Amplitude	Aspect Ratio	Skewness
--	--	[m]	[m]	--	--
1	0.09	580	16	37	0.24
2	0.21	840	59	14	-0.42
3	0.29	486	20	24	-0.35
4	0.36	702	35	20	-0.13
5	0.47	790	28	29	-0.51
6	0.52	338	16	21	-0.02
7	0.58	651	42	15	-0.02
8	0.68	487	6	85	-0.54
9	0.74	559	26	22	-0.41
10	0.78	306	8	37	0.14
11	0.85	822	22	37	0.22
12	0.94	274	8	33	-0.36
13	0.98	337	9	38	-0.21
Mean	**0.58**	**552**	**23**	**32**	**-0.18**
Std	**0.28**	**201**	**15**	**18**	**0.27**
Kurt	**-1.04**	**-1.39**	**1.18**	**6.59**	**-1.34**

Table 9 - Siletz sub-cell 2002

Embayment	Relative Location	Length	Amplitude	Aspect Ratio	Skewness
--	--	[m]	[m]	--	--
1	0.07	383	13	30	0.38
2	0.27	324	9	36	0.44
3	0.35	546	26	21	-0.33
4	0.47	353	17	21	-0.04
5	0.53	478	13	37	-0.24
6	0.60	443	10	44	0.33
7	0.68	410	9	48	-0.59
8	0.72	666	23	28	0.30
9	0.84	293	7	44	-0.32
10	0.89	553	23	24	-0.07
Mean	**0.54**	**445**	**15**	**33**	**-0.01**
Std	**0.26**	**117**	**7**	**10**	**0.36**
Kurt	**-0.40**	**-0.29**	**-1.29**	**-1.56**	**-1.41**

B. Modeling

B.1. Bathymetric generation

Program derived by Matthew M. Dalon for use with Matlab 7.1

```
% Matthew Dalon
% June 2007
% Bathymetric generationof an idealized rup current embayment

clear
clc

%% Constants
xc=400; %Offshore extent of the embayment
zc=4;   %Depth embayments extends to
emwidth=575; %Width of embayment
% moff=.01;%zc/xc; %Slope offshore of the embayment
xoffb=800;%10/moff; %Off shore extent of matrix to a depth of 10
meters

%% Beach Profile = A*x^m
mbeach=.635; %non embayment exponent
np1=mbeach-.1; %Embayment center exponent
np2=mbeach+0.033;%Horn exponent

%% Calculate intersection of sin curve to create desired embayment
length
amp=(np2-np1)/2;
zbump=amp+np1;
ms1=asin((mbeach-zbump)/amp);
dummyx=[2.5*pi:.1:3.5*pi];
dummysin=amp*sin(dummyx)+zbump;
ms2=interp1(dummysin,dummyx,mbeach);
dum=[ms1 ms2];
hornext=((dum(2)-dum(1))-2*(asin((np2-zbump)/amp)-
      asin((mbeach-zbump)/amp)))/(dum(2)-dum(1));

%% Create the Grid
dx=5; dy=dx; %Grid Spacing
x=[0:dx:xc];
xoff=[xc+dx:dx:xoffb];
xall=horzcat(x,xoff);
y=[0:dy:emwidth/hornext]';
yext=emwidth/3;
yflat=[0:dy:yext]';
```

```
yall=[0:dy:2*max(yflat)+max(y)+2*dy]';

[X,Y]=meshgrid(xall,yall);
xygrid=vertcat(X,Y);

Zem=NaN(length(yall),length(x));
Zoff=NaN(length(yall),length(xoff));
Zall=NaN(length(yall),length(xall));
embayment=NaN(length(yall),length(xall));

%% Calculate exponent function for the length of the beach
nps=(dum(2)-dum(1))/(length(y)-1);
npc=[dum(1):nps:dum(2)];
n=amp*sin(npc)+zbump;
nall=ones(length(yall),1)*mbeach;
nall(yflat(end)/dy:yflat(end)/dy+y(end)/dy)=n;

%% Create the beach Z=A*X^n
for a=1:length(yall)
    A(a)=zc/xc^nall(a);
    ws(a)=(A(a)/(0.067)).^(1/.44);
    Zem(a,:)=A(a).*x.^nall(a);
    Zoff(a,:)=A(1).*xoff.^(nall(1));
end

Zall=horzcat(Zem,Zoff);
```

B.2. SHORECIRC Input Files

Indata.dat

```
&FNAMES
 FNAME2 = 'refdat.dat',
 FNAME3 = 'subdat.dat',
 FNAME4 = 'wave.dat',
 FNAME5 = 'refdif1.log',
 FNAME6 = 'height',
 FNAME7 = 'angle.dat',
 FNAME8 = 'dep.dat',
 FNAME9 = ' ',
 FNAME10 = ' ',
 FNAME11 = ' ',
 FNAME12 = ' ',
 FNAME13 = ' ',
 FNAME14 = ' ',
 FNAME15 = ' ',
 FNAME16 = ' ',
 FNAME17 = ' ',
 FNAME18 = ' ',
 FNAME19 = ' ',
 FNAME20 = 'owave.dat',
 FNAME21 = ' ',
 FNAME22 = ' ',
 FNAME23 = ' ',
 FNAME24 = ' ',
 FNAME25 = ' ',
 FNAME26 = ' ',
/
&INGRID
 MR = 161,
 NR = 232,
 IU = 1,
 NTYPE = 0,
 ICUR = 0,
 IBC = 1,
 ISMOOTH = 1,
 DXR =  5.,
 DYR =  5.,
 DT =  10.,
 ISPACE = 0,
 ND = 1,
 IFF = 0 0 1,
 ISP = 0,
 IINPUT = 1,
 IOUTPUT = 1/
&WAVES1A
 IWAVE= 1,
```

```
 NFREQS = 1/
&WAVES1B
 FREQS = 9.,
 TIDE = 0,
 NWAVS = 1,
 AMP = 1.0001,  (input 0.5, 1, 1.5)
 DIR = 0/
```

Input_winc.dat

```
&BOUNDARY
 IBC1 = 2,
 IBC2 = 4,
 IBC3 = 5,
 IBC4 = 5/
&GRIDS
 DX =  5.,
 DY =  5.,
 NX = 161,
 NY = 232,
 NXWALL = 159,
 HTTIDE = 0.00/
&SHORT_WAVE
 PERIOD =  10.,
 WC = 0,
 AMERGE = 10/
&CONTROL
 CR = 0.5,
 NTIME = 101,
 INTERVAL = 1,
 KOLD_START = 1,
 DEPTHMIN =  0.04,
 DELAY =  20/
&SENSOR
 JUMP = 10,
 XSENSOR = 120 0 0 0 0 0 0 0 0 0 0 0 0 0 0 0 0 0 0 0 0 0,
 YSENSOR = 120 0 0 0 0 0 0 0 0 0 0 0 0 0 0 0 0 0 0 0 0 0,
 YPROFILE = 110 0 0 0 0 0 0 0 /
&OUTPUTSC
 TAVGOUT = 1,
 MOMOUT = 1,
 DISPOUT = 1/
&PHYSICS
 FCW = 0.0071,
 VTSHEAR = 0.08,
 MDISS = 0.1,
 CS = 0.2,
 WIND_VEL = 0.,
 WIND_DIR = 0.,
 DISP3D = 1/
```

Minput.dat

```
&F_NAMES
 F_depth = 'depth.dat',
 F_xymast = 'xymast.dat'
 F_xywave = ' ',
 F_xycirc = ' ',
 F_xysedi = ' ',
 F_NAME6 = ' ',
 F_NAME7 = ' ',
 F_NAME8 = ' ',
 F_NAME9 = ' ',
 F_NAME10 = ' ',
 F_NAME11 = ' ',
 F_NAME12 = ' ',
 F_NAME13 = 'wheight.out ',
 F_NAME14 = 'cu.out',
 F_NAME15 = 'cv.out',
 F_NAME16 = 'ceta.out'/
&GRIDIN
 Nx_Mast = 161,
 Ny_Mast = 232,
 Nx_Circ = 161,
 Ny_Circ = 232,
 Nx_Wave = 161,
 Ny_Wave = 232,
 Nx_Sedi = 161,
 Ny_Sedi = 232,
 Grid_Mast_Wave_Same = .true.,
 Grid_Mast_Circ_Same = .true.,
 Grid_Mast_Sedi_Same = .true.,
 Wave_Staggered = .false.,
 Wave_Stag_huv = 0 0 0,
 Circ_Staggered = .false.,
 Circ_Stag_huv = 0 0 0,
 Sedi_Staggered = .false.,
 Sedi_Stag_huv = 0 0 0,
 Wave_Structured = .true.,
 Circ_Structured = .true.,
 Sedi_Structured = .true.,
 Grid_Extrapolation = .false.,
/
&INTERACTION
 Wave_Curr_Interact = .true.,
 Wave_Bed_Interact = .true.,
 Curr_Bed_Interact = .true.,
/
```

```
&PASSVARIABLES
 Wave_To_Circ_Height = .true.,
 Wave_To_Circ_Angle = .true.,
 Wave_To_Circ_WaveNum = .true.,
 Wave_To_Circ_C = .true.,
 Wave_To_Circ_Radiation = .true.,
 Wave_To_Circ_Rad_Surf = .false.,
 Wave_To_Circ_Rad_Body = .false.,
 Wave_To_Circ_Forcing = .false.,
 Wave_To_Circ_MassFlux = .true.,
 Wave_To_Circ_Dissipation = .true.,
 Wave_To_Circ_BottomUV = .true.,
 Wave_To_Circ_Brkindex = .true.,
 Circ_To_Wave_UV = .true.,
 Circ_To_Wave_eta = .true.,
 Wave_To_Sedi_Height = .true.,
 Wave_To_Sedi_Angle = .true.,
 Wave_To_Sedi_BottomUV = .true.,
 Circ_To_Sedi_UV = .true.,
 Circ_To_Sedi_UVb = .true.,
 Circ_To_Sedi_eta = .true.,
 Circ_To_Sedi_UV3D = .false.,
 Circ_To_Sedi_fw = .true.,
 Circ_To_Sedi_UVquasi3D = .false.,
 Sedi_To_Wave_Depth = .true.,
 Sedi_To_Circ_Depth =.true.,
/
&VECTORROTATE
 Circ_Rotate_Angle = 0.,
 Wave_Rotate_Angle = 0.,
 Sedi_Rotate_Angle = 0.,
/
&TIMEIN
 Total_Time = 5000,
 Master_dt = 20.,
 N_Interval_CallWave = 5000,
 N_Interval_CallCirc = 1,
 N_Interval_CallSedi = -1,
 N_Delay_CallSedi =1,
 N_Interval_Output = 20,
/
```